CNS myelin induces regulatory functions of DC-SIGN–expressing, antigen-presenting cells via cognate interaction with MOG

J.J. García-Vallejo,[1] J.M. Ilarregui,[1] H. Kalay,[1] S. Chamorro,[1] N. Koning,[1] W.W. Unger,[1] M. Ambrosini,[1] V. Montserrat,[2] R.J. Fernandes,[1] S.C.M. Bruijns,[1] J.R.T. van Weering,[3] N.J. Paauw,[1] T. O'Toole,[1] J. van Horssen,[1,4] P. van der Valk,[4] K. Nazmi,[5] J.G.M. Bolscher,[5] J. Bajramovic,[6] C.D. Dijkstra,[1] B.A. 't Hart,[7,8] and Y. van Kooyk[1]

[1]Department of Molecular Cell Biology and Immunology, VU University Medical Center, 1081HV Amsterdam, Netherlands
[2]Division of Cell Biology, Dutch Cancer Institute, 1066X Amsterdam, Netherlands
[3]Department of Functional Genomics and Clinical Genetics, Center for Neurogenomics and Cognitive Research, Neuroscience Campus Amsterdam; and [4]Department of Pathology, VU University Amsterdam, VU University Medical Center, 1081HV Amsterdam, Netherlands
[5]Department of Oral Biochemistry, Academic Centre for Dentistry Amsterdam, University of Amsterdam, VU University, 1081LA Amsterdam, Netherlands
[6]Alternatives Unit and [7]Dept. Immunobiology, Biomedical Primate Research Centre, 2280 GH Rijswijk, Netherlands
[8]Department Neuroscience, University Medical Center, University of Groningen, 9713GZ Groningen, Netherlands

Myelin oligodendrocyte glycoprotein (MOG), a constituent of central nervous system myelin, is an important autoantigen in the neuroinflammatory disease multiple sclerosis (MS). However, its function remains unknown. Here, we show that, in healthy human myelin, MOG is decorated with fucosylated *N*-glycans that support recognition by the C-type lectin receptor (CLR) DC-specific intercellular adhesion molecule-3–grabbing nonintegrin (DC-SIGN) on microglia and DCs. The interaction of MOG with DC-SIGN in the context of simultaneous TLR4 activation resulted in enhanced IL-10 secretion and decreased T cell proliferation in a DC-SIGN–, glycosylation–, and Raf1-dependent manner. Exposure of oligodendrocytes to proinflammatory factors resulted in the down-regulation of fucosyltransferase expression, reflected by altered glycosylation at the MS lesion site. Indeed, removal of fucose on myelin reduced DC-SIGN–dependent homeostatic control, and resulted in inflammasome activation, increased T cell proliferation, and differentiation toward a Th_{17}-prone phenotype. These data demonstrate a new role for myelin glycosylation in the control of immune homeostasis in the healthy human brain through the MOG–DC-SIGN homeostatic regulatory axis, which is comprised by inflammatory insults that affect glycosylation. This phenomenon should be considered as a basis to restore immune tolerance in MS.

CORRESPONDENCE
Y. van Kooyk:
y.vankooyk@vumc.nl

Abbreviations used: CLR, C-type lectin receptor; CNS, central nervous system; DC-SIGN, DC-specific intercellular adhesion molecule-3-grabbing nonintegrin; MOG, myelin oligodendrocyte glycoprotein; MS, multiple sclerosis; T reg cell, regulatory T cell.

Professional APCs are equipped with receptors that recognize, capture, and internalize antigens to facilitate their processing and presentation to T cells. Among APCs, DCs are unique in their capacity to stimulate naive T cells; however, their function is not restricted to the initiation of strong immune responses against pathogens, but also to regulate T cell homeostasis and prevent autoimmunity. Indeed, DCs efficiently support the in vitro generation and expansion of iT reg cells, regulate T reg cell homeostasis in vivo (Fehérvári and Sakaguchi, 2004; Cong et al., 2005), and even induce T cell anergy (Hawiger et al., 2001). Targeting of antigen to resting DCs via DEC-205 resulted in an unsustained

Dr. Chamorro died in March of 2014.

N. Koning's present address is Excerpta Medica, Amsterdam, Netherlands.

V. Montserrat's present address is Dept. Immunohematology and Blood Transfusion, Leiden University Medical Center, Leiden, Netherlands.

The Rockefeller University Press $30.00
J. Exp. Med. 2014 Vol. 211 No. 7 1465-1483
www.jem.org/cgi/doi/10.1084/jem.20122192

expansion of antigen-specific $CD4^+$ T cells that did not differentiate into effector cells (Hawiger et al., 2001). Similar functional unresponsiveness was observed in naive antigen-specific $CD8^+$ T cells when splenic lymphoid DCs were exposed to dying cells loaded with cognate antigen (Liu et al., 2002). Unfortunately, reports on DC-lacking mice are controversial (Birnberg et al., 2008; Ohnmacht et al., 2009) and the precise role of DCs in the maintenance of peripheral tolerance in humans remains to be determined.

C-type lectin receptors (CLRs), such as DEC-205 and DC-specific intercellular adhesion molecule-3–grabbing nonintegrin (DC-SIGN), have been proposed to play an important role in homeostatic control. DC-SIGN is a type II transmembrane receptor equipped with a Ca^{2+}-dependent mannose-binding carbohydrate recognition domain with specificity for antigens decorated with high-mannose or Lewis-type structures (Appelmelk et al., 2003). Signaling crosstalk with TLRs has been demonstrated for DC-SIGN and some other CLRs on DCs (Geijtenbeek and Gringhuis, 2009). Although eight mouse genetic homologues are known (Park et al., 2001; Powlesland et al., 2006), none has the same glycan specificity, expression profile, or signaling properties as human DC-SIGN (García-Vallejo and van Kooyk, 2013). Hence, knowledge on the physiological functions of DC-SIGN is based on human in vitro data. Contrary to other antigen-uptake receptors, pathogen recognition by DC-SIGN often results in immune escape (van Kooyk and Geijtenbeek, 2003; Rappocciolo et al., 2008; Wang et al., 2008) and the carbohydrate ligands of DC-SIGN are also found on host glycoproteins, suggesting that DC-SIGN participates in the control of immune homeostasis (García-Vallejo and van Kooyk, 2009). Interaction of DC-SIGN with its ligands on immune cells mediates adhesion and favors communication during (cognate) interactions. DC-SIGN ligands on nonimmunological tissues, such as the tumor-associated epithelial proteins CEA and CEACAM1 (van Gisbergen et al., 2005) can enhance the cytokine response of DCs to the TLR4 ligand LPS in a similar way, as previously reported for the *M. tuberculosis* DC-SIGN ligand ManLAM, by synergistically increasing the LPS-mediated secretion of IL-10 (Geijtenbeek et al., 2003). Additionally, supernatants from CEA and CEACAM1-producing cell lines inhibited DC maturation and attenuated Th_1 skewing (Nonaka et al., 2008). Apparently, both tumor and pathogens have ways to escape immune activation by targeting a receptor that is able to transform proinflammatory into tolerogenic signals. DC-SIGN has therefore been proposed to be a homeostatic receptor that can be subverted by pathogens and tumors through changes in their glycan phenotype. However, DC-SIGN has not yet been found to recognize any autoantigen, or to support any role in the maintenance of peripheral tolerance in humans.

The central nervous system (CNS) has evolved as an immune-privileged site to protect its vital functions from detrimental insults, by immune-mediated inflammation. Microglia are CNS-based APCs that continuously evaluate local changes in the CNS to activate the immune system during injury (Olson and Miller, 2004) or to maintain homeostasis in the steady state (Lambert et al., 2008). Accumulating evidence suggests that glycosylation plays a role in the control of peripheral tolerance to brain autoantigens. Induction of experimental autoimmune encephalomyelitis, the animal model of MS, is much more efficient when recombinant unglycosylated myelin oligodendrocyte glycoprotein (MOG) is used, in contrast to native MOG (Smith et al., 2005). Also, alterations in glycosyltransferases (Husain et al., 2008; Brynedal et al., 2010) or glycan-binding proteins (Hoppenbrouwers et al., 2009) have been linked to a higher incidence of MS. Yet, the molecular mechanisms behind this association remain unclear.

Here, we show for the first time that a major autoantigen in MS, MOG, is recognized by DC-SIGN on APCs within the human brain, including microglia. The interaction results in the transmission of a tolerogenic signal characterized by increased IL-10 secretion and decreased T cell proliferation. Conversely, myelin particles lacking DC-SIGN ligands induce immunogenic signals characterized by inflammasome activation and enhanced T cell proliferation. Our results help to explain how an immunosuppressive milieu in the healthy human CNS is maintained through the glycosylation status of MOG/myelin that engages DC-SIGN, keeping local APCs in an immature nonpathogenic state.

RESULTS

DC-SIGN is expressed on microglia in the resting human brain

DC-SIGN has been classically described as a human DC marker in peripheral tissues, such as skin and mucosa, and in lymphoid organs (Soilleux et al., 2002; Engering et al., 2004). In the brain, DC-SIGN is expressed on $CD163^+$ perivascular macrophages (Fabriek et al., 2005a), meningeal DCs (Serafini et al., 2006), and in vitro–cultured microglia (Lambert et al., 2008). Using the polyclonal antibody CSRD against the C terminus of DC-SIGN (Engering et al., 2004), as well as two mAbs against the stalk region of DC-SIGN, we sought to determine if DC-SIGN is expressed in normal human brain. Immunohistochemical analysis demonstrated a pattern of $DC\text{-}SIGN^+$ small cells scattered throughout the brain parenchyma, with little perinuclear cytoplasm and branched processes covered with fine protrusions (Fig. 1 a, arrows), being distinctive features of microglia. Preblocking CSRD with recombinant soluble DC-SIGN completely abolished staining, verifying antibody specificity (Fig. 1 b). Relatively large cells within perivascular spaces were also stained, suggestive of perivascular macrophages (Fig. 1 b, arrow). Colocalization of DC-SIGN and HLA-DR, a constitutive marker of microglia, confirmed the identity of these cells as microglia (Fig. 1 c). Moreover, high levels of DC-SIGN could be demonstrated on primary human microglia ($MHC\text{-}II^+CD11c^+GSL\text{-}I$ isolectin B_4^+) isolated from a surgical brain biopsy (Fig. 1 d). Expression of DC-SIGN at the transcript level could also be demonstrated in microglia isolated from cryosections by laser-capture microdissection of $MHC\text{-}II^+$ cells and also in primary microglia from human brain tissue (Fig. 1 e). DC-SIGN transcripts were considerably less abundant in microglia

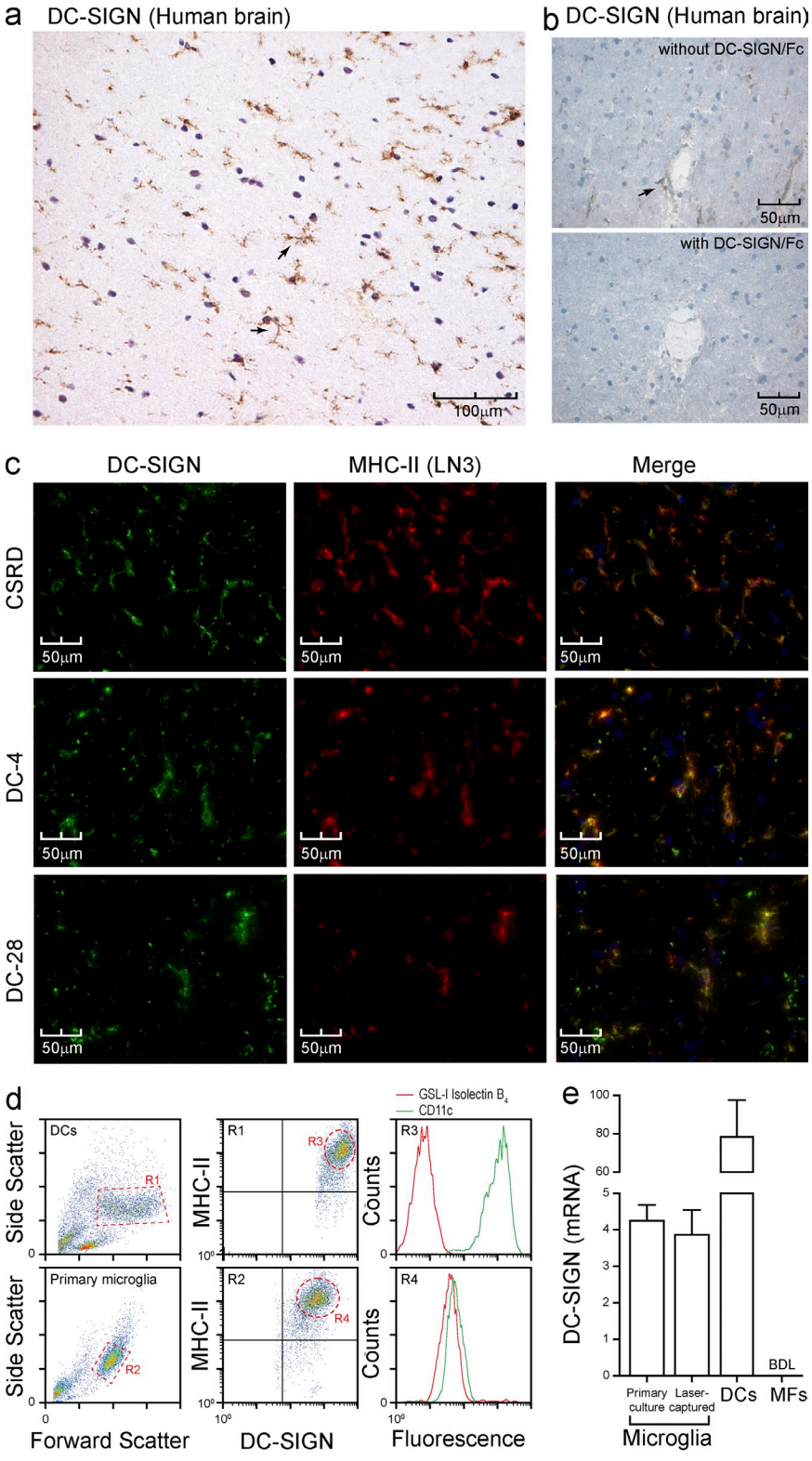

Figure 1. DC-SIGN is expressed on microglia. (a) Frozen healthy human brain sections were stained for DC-SIGN with the polyclonal antibody CSRD and imaged by immunohistochemistry. Arrows highlight typical microglia features (representative of $n > 7$ donors). (b) Frozen healthy human brain sections were stained for DC-SIGN with CSRD with or without recombinant DC-SIGN and imaged by immunohistochemistry. The arrow highlights a perivascular macrophage (representative of $n > 7$ donors). (c) Frozen healthy human brain sections were stained for DC-SIGN (green) and MHC-II (red) and imaged by immunofluorescence microscopy. Three different anti–DC-SIGN antibodies were used: CSRD (polyclonal), DC-4 and DC-28 (mAbs against the stalk region; representative of $n > 7$ donors). (d) Primary microglia were isolated from a brain biopsy; stained for DC-SIGN, MHC-II, CD11c, and GSL-I Isolectin B_4; and analyzed by FACS. DCs were analyzed in parallel for comparison (representative of triplicate determination). (e) DC-SIGN transcripts were quantified by real time RT-PCR after laser-capture microdissection of MHC-II$^+$ cells from frozen normal brain sections (pool of 3 donors) and primary microglia as in d. Data are the mean ± SD ($n = 3$ independent experiments). BDL, below detection limit.

as compared with DCs (Fig. 1 e). As expected, macrophages did not express DC-SIGN (Fig. 1 e). Primary microglia and laser-captured MHC-II$^+$ cells were negative for the astrocyte marker GFAP and the perivascular macrophage marker CD163 (unpublished data). These data demonstrate that DC-SIGN is expressed on both microglia and perivascular macrophages in healthy human brain, closely associated with highly myelinated areas.

DC-SIGN recognizes glycan structures on human healthy myelin

To investigate the functional implications of DC-SIGN expression on APCs within the brain, we isolated myelin from healthy human brain by a sucrose gradient centrifugation (Fig. 2 a). The particles generated with this protocol contained the myelin proteins MOG and PLP and lacked other cell-type markers (Fig. 2 b). Further characterization by electron microscopy showed that myelin particles adopt a liposome-like shape of heterogeneous size distribution,

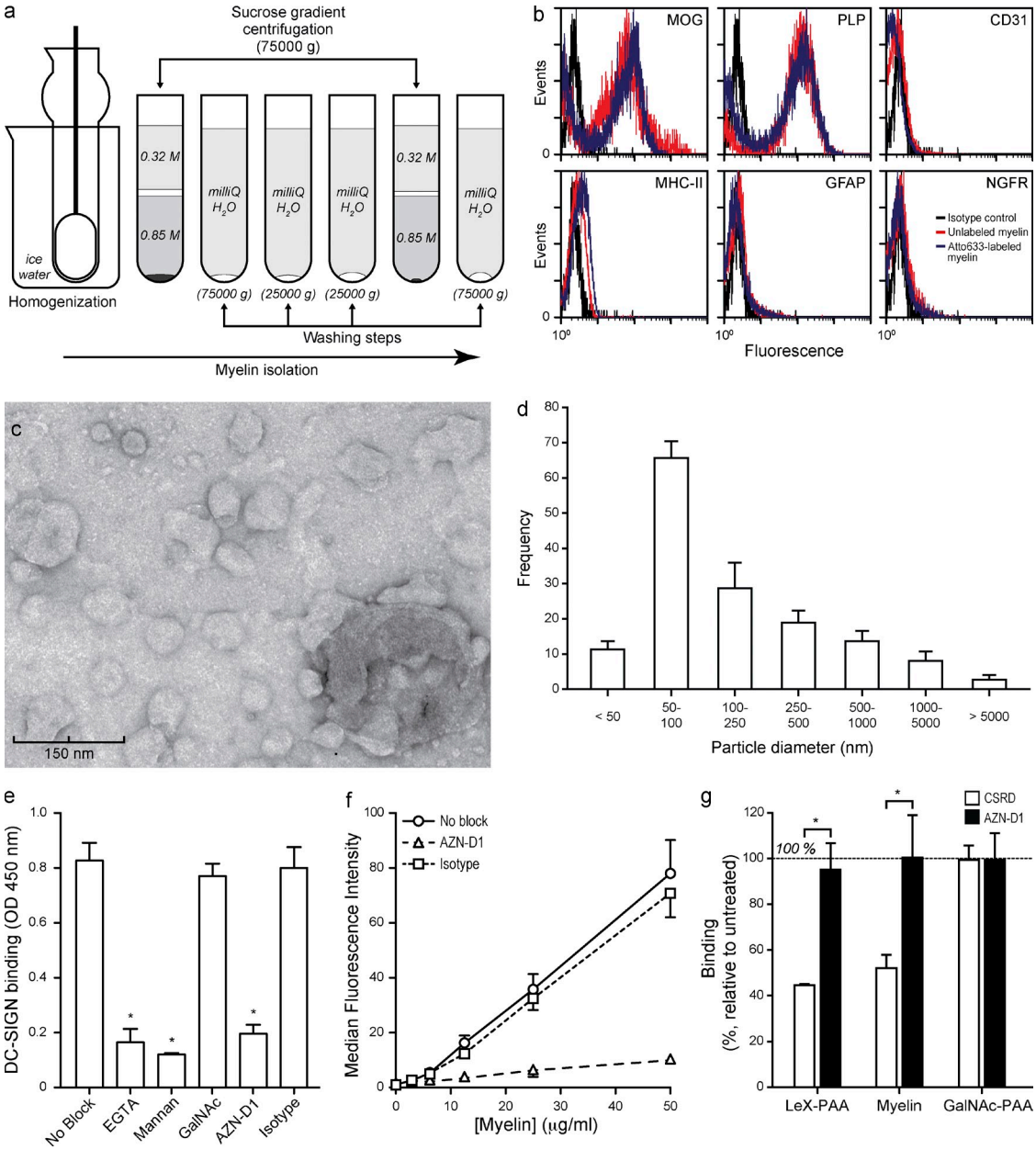

Figure 2. Characterization of human myelin. (a) Myelin was prepared by homogenization of fresh human white matter and sucrose gradient centrifugation, as indicated in the scheme. (b) The resulting myelin particles were characterized by FACS using microglial (MOG and PLP), endothelial (CD31), microglial (MHC-II), astrocytic (GFAP) or neuronal (NGFR) markers (representative of $n > 3$ donors). (c) Transmission electron micrograph of myelin particles (representative of $n > 3$ donors). (d) The diameter of 100 myelin particles was measured in 10 different micrographs. Data are the mean ± SD ($n = 3$ independent experiments). (e) Myelin was coated on to ELISA plates and the binding of DC-SIGN measured by a DC-SIGN–binding assay as described in the Materials and methods. *, $P \leq 0.05$ (Mann-Whitney *U* test). Data are the mean ± SD ($n = 3$ independent experiments). (f) Binding of a titration of atto633-labeled myelin to DC-SIGN–expressing DCs was measured by FACS. Data are the mean ± SD ($n = 3$ independent experiments). (g) DCs were incubated with myelin (10 µg/ml), the DC-SIGN ligand PAA-Le^X (10 µg/ml), or the MGL-ligand PAA-GalNAc (10 µg/ml), washed, and fixated. Binding of the DC-SIGN–specific antibodies AZN-D1 (mAb against carbohydrate-recognition domain) and CSRD (polyclonal against C terminus) was determined by FACS. Data are shown as the mean ± SD ($n = 3$ independent experiments).

with 50–100 nm as the most frequent particle diameter (Fig. 2, c and d).

Because DC-SIGN has been shown to recognize ligands on both self- and nonself-glycoproteins, we decided to explore the presence of DC-SIGN ligands on myelin using an ELISA-based DC-SIGN–binding assay. Results indicate that DC-SIGN binds to myelin in a Ca^{2+}-dependent manner (Fig. 2 e), as expected for a CLR. Furthermore, binding could be blocked with the DC-SIGN ligand mannan or a blocking anti–DC-SIGN antibody (AZN-D1), but not with an irrelevant carbohydrate or an isotype control (Fig. 2 e). To investigate if myelin also binds cellular DC-SIGN, myelin particles were labeled with atto633 and binding to DCs was addressed by FACS. Results demonstrate that myelin was recognized by DCs in a concentration- and DC-SIGN–dependent manner, as the binding was completely inhibited by preincubation of DCs with the DC-SIGN blocking antibody AZN-D1 (Fig. 2 f).

A previous study using the mAb AZN-D1 failed to identify DC-SIGN expression on microglia (Fabriek et al., 2005a). However, using three different antibodies targeting DC-SIGN domains that are not involved in carbohydrate recognition, our data unequivocally demonstrate the presence of DC-SIGN on microglia. A plausible explanation for this controversy could be that the epitope of AZN-D1 on DC-SIGN (the carbohydrate recognition domain) is occupied by its ligand. To test this possibility, we incubated DCs with myelin particles or the well-known DC-SIGN ligand Le^X-PAA and subsequently stained the cells with either AZN-D1 or CSRD. Incubation with myelin particles or Le^X-PAA resulted in a similar decrease in AZN-D1 staining, whereas staining with CSRD was not affected at all (Fig. 2 g). These data suggest that DC-SIGN on healthy CNS microglia is engaged in continuous interaction with myelin.

To characterize the carbohydrate ligands of DC-SIGN we performed a quantitative glycan profiling of human CNS myelin (Fig. 3, a and b). Strikingly, the variety of Lewis-type antigen-containing glycans (α3/4-fucosylated branch structures) was unusually rich as compared with other tissues (http://www.functionalglycomics.org). The presence of highly fucosylated glycans was confirmed by lectin ELISA, as shown by the binding of the fucose-specific plant lectins LTA, UEA-I, and AAL, as well as with a $Lewis^X$-specific mAb (Fig. 3 c).

Glycosylation is often subjected to regulation by inflammatory mediators. To investigate if the glycosylation of myelin is sensitive to common proinflammatory mediators, we assessed the expression of the glycosyltransferases involved in the synthesis of DC-SIGN ligands on primary oligodendrocytes obtained from rhesus macaques exposed to TNF or IL-6. Rhesus macaque oligodendrocytes were used because of their close genetic proximity to humans. Treatment of primary oligodendrocytes with proinflammatory cytokines resulted in a marked down-regulation of the transcripts for the fucosyltransferases FUT-1 (GeneID: 2523) and FUT-4 (GeneID: 2526; Fig. 3 d). Similar results were obtained using the human oligodendrocyte cell line MO3.13 (unpublished data). These results indicate that proinflammatory agents affect the glycosylation of myelin by down-regulating fucosyltransferase expression on oligodendrocytes and, therefore, decreasing the amount of fucosylated DC-SIGN ligands on myelin glycoproteins.

MOG is a ligand for DC-SIGN on human myelin

Among the glycoproteins present in myelin that could support DC-SIGN binding, we speculated that MOG could be an interesting candidate. MOG is a type I membrane homodimer on the outermost surface of the myelin sheath. Both glycans on the homodimer (Asn_{31}) are localized to the top of the structure (Clements et al., 2003). The close proximity of both glycans in the dimer and the presence of MOG in lipid rafts (Kim and Pfeiffer, 1999) suggest that MOG-rich microdomains could display their glycans in multivalent form, providing a potentially high-avidity binding platform for carbohydrate-binding proteins. Because the glycosylation of MOG has been poorly characterized we first set out to investigate the glycan composition of MOG. For this purpose, MOG was immunoprecipitated using the mAb Z12 and its glycans were sequenced. The majority of the glycans identified contained one or two terminal fucoses, corresponding to the typical Lewis-type DC-SIGN ligands already described on myelin (unpublished data).

To investigate whether MOG is involved in interactions with DC-SIGN, we tested the binding of soluble DC-SIGN to myelin isolated from brains of C57BL/6 WT and $Mog^{-/-}$ mice by FACS. Results clearly show that DC-SIGN binds to WT myelin but not to $Mog^{-/-}$ myelin, indicating that MOG is the sole ligand of DC-SIGN on myelin (Fig. 3, e and f).

To study if the interaction of MOG and DC-SIGN is glycosylation-dependent, we expressed MOG on Lec12 cells, which overexpress Lewis-type glycans due to a gain-of-function mutation in FUT-IX (Patnaik et al., 2004), or CHO cells, which lack Lewis-type glycans (North et al., 2010). MOG expression in both cell lines was verified by staining with the MOG-specific mAb Z12 (Fig. 3 g). A sandwich ELISA was then designed using Z12 as a capture antibody and recombinant soluble DC-SIGN for detection. Results demonstrate that only MOG modified with fucosylated glycans binds DC-SIGN (Fig. 3 h). These data demonstrate that human MOG is a ligand for DC-SIGN when properly glycosylated.

DC-SIGN interacts only with large myelin particles and mediates internalization

As shown in Fig. 2 (c and d), myelin particles adopt liposome-like structures in a large range of size and complexity. Interestingly, only large myelin particles display high levels of MOG, bind the α(1–3, 4)fucose-specific plant lectin LTA, and are able to bind soluble DC-SIGN (Fig. 4 a). Small myelin particles show hardly any MOG and no DC-SIGN binding, which is consistent with a lack of fucose as illustrated by the poor LTA staining (Fig. 4 a).

Differences in MOG expression and DC-SIGN binding related to the myelin particle size can be explained by the association of MOG to lipid rafts (Kim and Pfeiffer, 1999) which, because of their size (Simons and Vaz, 2004), are exclusively present in large myelin particles. Upon exposure to

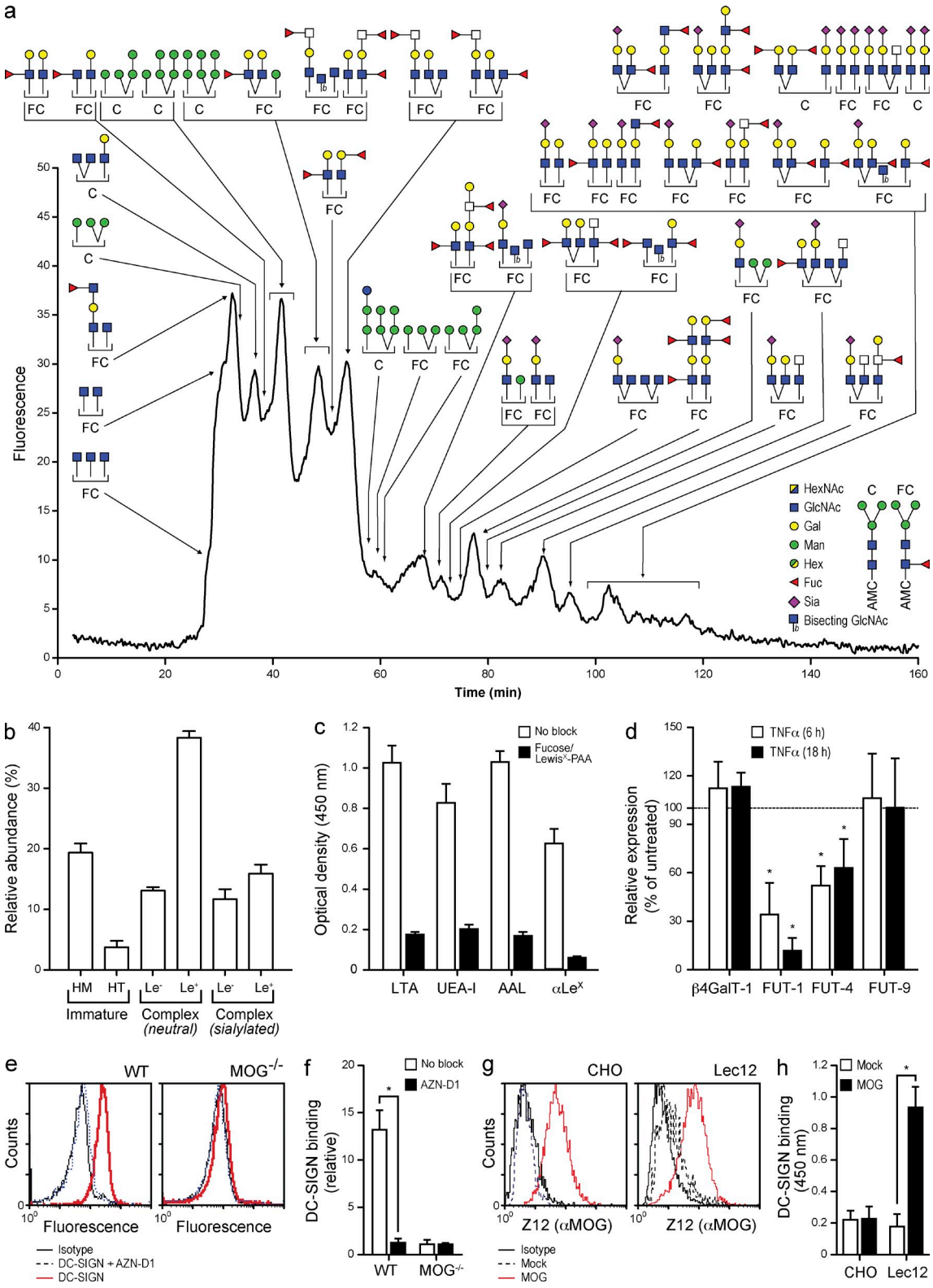

Figure 3. Myelin is rich in *N*-glycans carrying DC-SIGN–binding carbohydrates. (a) *N*-glycans were enzymatically released, purified, fluorescently labeled, and profiled by LC-MS. Data are representative of the profiles of three myelin preparations. (b) The relative distribution of the main categories of *N*-glycans; high-mannose (HM), hybrid-type (HT), and Lewis antigen (Le) containing complex type *N*-glycans, was determined in three myelin preparations. Data are shown as the mean ± SD ($n = 3$ independent experiments). (c) Myelin was coated on to plates and the binding of the fucose-specific plant lectins *Lotus tetragonolobus* (LTA) *Ulex europaeus* (UEA-I), and *Aleuria aurantia* (AAL) agglutinins, and a Lewis^X-specific mAb was measured by ELISA. Data

DC-SIGN–expressing APCs, myelin particles are quickly internalized. A fraction of DCs internalize exclusively the smaller myelin particles that cannot be detected by confocal microscopy, but can still be measured by FACS (My^{Lo}; Fig. 4 b). Importantly, some DCs accumulate large myelin particles, as determined by FACS and confocal microscopy of My^{Hi} FACS-sorted DCs (My^{Hi}; Fig. 4 b). Using FACS imaging, we investigated whether large myelin particles are internalized and if they followed the classical endolysosomal routing previously described for DC-SIGN (Engering et al., 2002; Cambi et al., 2009). Results demonstrate that the localization of myelin particles in My^{Hi} DCs is fully intracellular (Fig. 4 c) and that myelin colocalizes with DC-SIGN at an early time-point (Fig. 4 d) and with the lysosomal marker LAMP-1 after 1 h (Fig. 4, e and g). Furthermore, My^{Hi} DCs contain ∼18 myelin particles per cell, irrespective of co-incubation with LPS (Fig. 4 f). These data demonstrate that the interaction of DC-SIGN with large myelin particles leads to internalization and routing to the endolysosomal pathway. Interaction of small myelin particles with DCs is independent of DC-SIGN and presumably results in internalization via pinocytosis or other nonspecific mechanisms.

Interaction of myelin with DC-SIGN–expressing APCs modulates the LPS-mediated expression and secretion of IL-10

The interaction of DC-SIGN with its ligands is accompanied by signaling events (Caparrós et al., 2006; Gringhuis et al., 2007, 2009) that modify the response of DCs to LPS. To investigate if myelin binding triggers such responses, we first addressed the presence of LPS in our myelin preparation using a HEK293-TLR4-CD14 transfected cell line that secretes IL-8 upon triggering of TLR4 (Latz et al., 2002). All myelin preparations were devoid of TLR4 ligands (Fig. 5 a). We then exposed DCs to myelin in the presence or absence of the well-characterized TLR4 ligand LPS and analyzed the expression of IL-1β, IL-6, IL-8, IL-10, IL12p35, IL-12p40, IL-18, IL-23p19, EBI3, IL-33, TNF, and TGFβ (Fig. 5, b–m). Interestingly, stimulation with both myelin and LPS resulted in a synergistic increase in the expression of IL-10 (Fig. 5 e) and had no effect on other cytokines. To test whether myelin triggered DC maturation, the expression levels of CD80, CD83, CD86, and MHC-I and MHC-II were investigated by FACS. Incubation of DCs with myelin with or without LPS did not affect the expression profile of any of the assayed markers (unpublished data). We also investigated if myelin interfered with signaling pathways other than TLR4, such as IFNγR1, IL-6R, or IL-17R. However, with the exception of LPS, none of the stimuli tested in combination with myelin had any effect on the expression of IL-10 (Fig. 5 n).

The three-dimensional orientation of MOG *N*-glycans and the enrichment of MOG homodimers in lipid rafts contribute to highly multivalent DC-SIGN ligands on myelin. The presentation of glycan epitopes in high density and number are important determinants of the binding and effector functions of lectins (Dam and Brewer, 2010). To investigate if the interaction of DC-SIGN with its carbohydrate ligand is positively influenced by multivalency, we designed glycodendrimers carrying a typical fucose-containing DC-SIGN ligand (Le^b), similar to those present on MOG and myelin. Incubation of the DC-SIGN–expressing DCs with Le^b glycodendrimers did not affect the expression of co-stimulatory molecules and maturation markers or the expression and secretion of cytokines (unpublished data). However, when DCs were exposed to Le^b glycodendrimers in the presence of the TLR4 ligand LPS we observed an effect that was similar to that of myelin, namely a synergistic increase in the expression (not depicted) and secretion of the antiinflammatory cytokine IL-10 (Fig. 6 a), whereas none of the other cytokines were affected (not depicted). We further verified that the synergistic increase in IL-10 expression upon simultaneous stimulation with myelin and LPS resulted also in a synergistic increase in IL-10 secretion (Fig. 6 b), but did not have any effect on the secretion of other cytokines such as IL-1β, IL-6, IL-8, IL-12p70, IL-23, TNF, or TGFβ (not depicted). Since only My^{Hi} DCs are affected by the interaction of DC-SIGN with its ligands on myelin, we hypothesized that only My^{Hi} DCs could synergistically increase IL-10 expression upon simultaneous incubation with myelin and LPS. To test this, we exposed DCs to atto633-labeled myelin with or without LPS and sorted the DCs according to myelin content. As expected, only large myelin particles modulated the signaling elicited by LPS on DCs, supporting the hypothesis that multivalency enhances DC-SIGN binding and functionality (Fig. 6 c). This phenomenon may have an in vivo correlate, as the $DC\text{-}SIGN^+$ cells in human normal brain also express IL-10 (Fig. 6 d), presumably as a result of the triggering of DC-SIGN by its myelin ligand MOG. In conclusion, our data demonstrate that DC-SIGN-mediated binding of myelin to DCs in the context of TLR4 ligation results in selective up-regulation of IL-10 expression and secretion, both in vitro and in vivo.

are shown as the mean ± SD (*n* = 3 independent experiments). (d) Primary oligodendrocytes were freshly isolated from rhesus macaques and cultured in the presence of TNF (100 IU/ml) for up to 18 h. The expression levels of the glycosyltransferases involved in the synthesis of Lewis-type epitopes were determined by real time PCR. *, P ≤ 0.05 (Mann-Whitney *U* test). Data are shown as the mean ± SD (*n* = 3 independent experiments). (e and f) The binding of DC-SIGN to myelin from WT or $MOG^{-/-}$ C57Bl6 mice was determined by FACS. (g) Representative of three independent experiments. (h) Mean ± SD of the relative binding. *, P ≤ 0.05 (Mann-Whitney *U* test; *n* = 3 independent experiments). (g) A human full-length MOG construct was expressed on CHO cells or a glycosylation mutant (Lec12). The expression of MOG was verified by FACS using the mAb Z12. Representative of three independent experiments. (h) MOG was captured on Z12-coated plates and DC-SIGN binding was assessed by ELISA. Data are shown as the mean ± SD. *, P ≤ 0.05 (Mann-Whitney *U* test; *n* = 3 independent experiments).

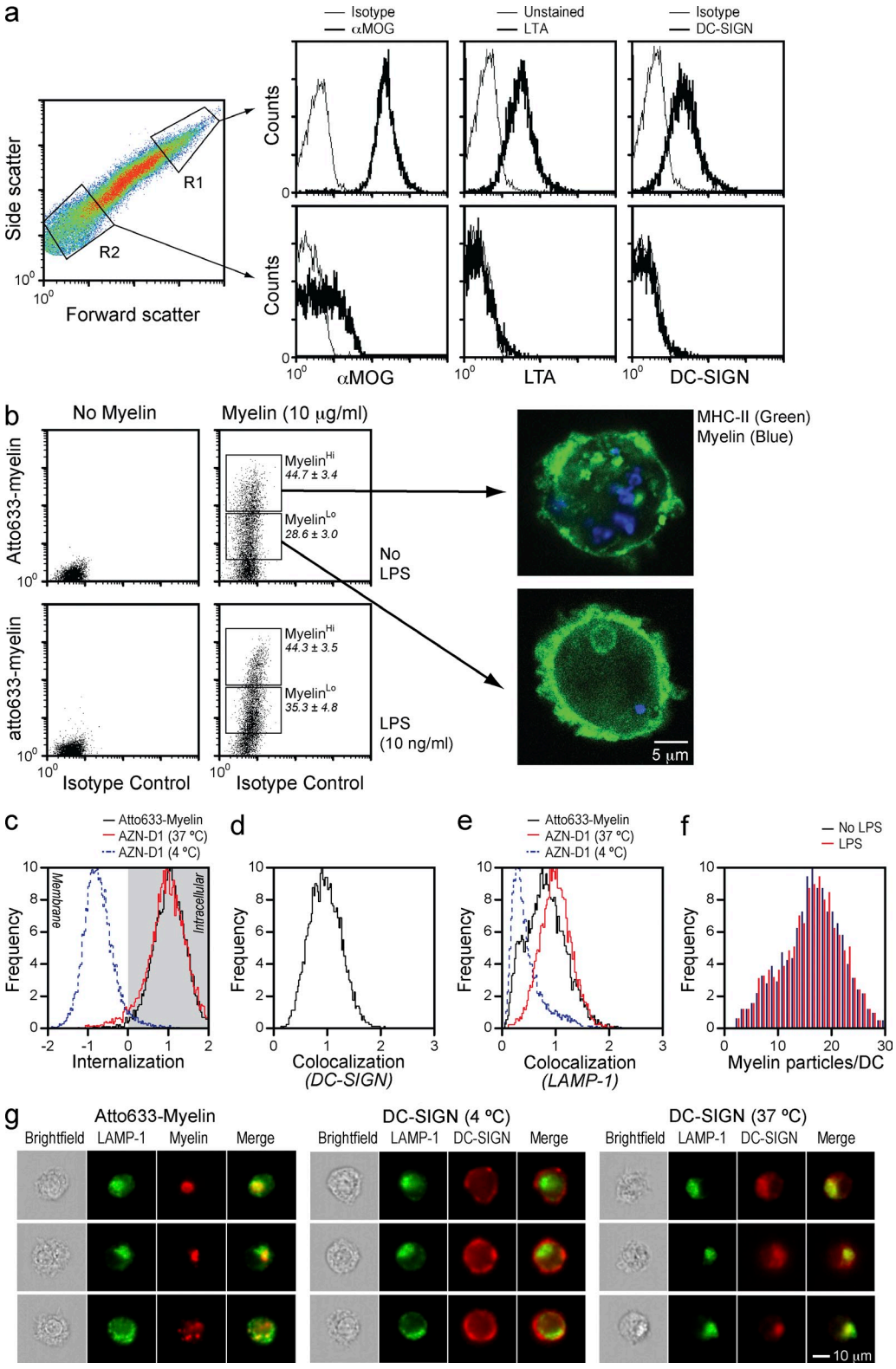

Figure 4. DC-SIGN mediates internalization and endolysosomal routing of large myelin particles. (a) Myelin particles were gated into large (R1) and small (R2) myelin particles and the level of MOG, and the presence of *Lotus tetragonolobus* agglutinin (LTA)-reactive structures (fucosylated glycans) and DC-SIGN ligands were addressed. Data are representative of three independent experiments. Thick lines represent cells stained with αMOG, the LTA lectin, or soluble DC-SIGN, whereas thin lines represent the corresponding isotype or unstained controls. (b) DCs were exposed to atto633-labeled myelin (10 μg/ml) for 1 h in the presence or absence of the TLR4 ligand LPS (10 ng/ml) and washed, and then the binding and uptake of myelin was measured by

We further investigated the presence of DC-SIGN$^+$ cells and fucosylated glycans in MS active lesions (Fig. 6, e–j). Interestingly, the demyelinated area corresponding to an MS lesion was rich in DC-SIGN$^+$ cells (Fig. 6 h), which appeared as foamy macrophages (Fig. 6 i), a phenotype previously associated to antiinflammatory functions (Boven et al., 2006). Moreover, intact myelin showed a PLP-like staining for LTA (Fig. 6 f) and Lewis^X-containing glycans (Fig. 6 g), whereas the center of the lesion was rich in a dense network of reactive astrocytes that were strongly positive for LTA (Fig. 6 f) and αLewis^X (Fig. 6 g). To investigate if astrocytes also express DC-SIGN ligands, we studied the binding of DC-SIGN to primary human astrocytes in vitro. Results demonstrate that, although astrocytes were rich in fucosylated structures that commonly serve as ligands for DC-SIGN, DC-SIGN was unable to bind these cells (Fig. 6 k). Incubation of astrocytes with high concentrations of TNF and IFN-γ, which results in a reactive phenotype (Sofroniew, 2009), significantly enhanced their fucosylation, but failed to induce any DC-SIGN binding (Fig. 6 l), probably due to a concomitant increase in sialylation that may result in the capping or masking of any potential DC-SIGN ligands and/or the absence of a proper protein scaffold for the carbohydrate ligands of DC-SIGN. Together with Fig. 3 (g–h), these data demonstrate that DC-SIGN binding requires not only a certain glycosylation, but also a specific protein scaffold, in this case MOG, reinforcing the importance of this glycoprotein as DC-SIGN ligand.

The combination of myelin and a TLR4 ligand triggers tolerogenic signaling on DCs

High IL-10 expression and secretion is the hallmark of tolerogenic APCs. Therefore, we investigated the effect of myelin or Le^b glycodendrimers exposure on T cell proliferation in a secondary MLR. CD4$^+$ T cells exposed to DCs pulsed with myelin or Le^b glycodendrimers showed decreased capacity to proliferate in response to a second stimulation with fully activated DCs (Fig. 7, a and b). This was interpreted as the induction of anergic T cells or T reg cells during the primary MLR. As expected, sorted My^{Hi} DCs induced generation of anergic/suppressor T cells (Fig. 7 c). These data indicate that recognition of myelin glycans by DC-SIGN expressing APCs can induce tolerance under inflammatory conditions through the induction of IL-10 and T cells with suppressor/inhibitory capacity.

To test whether the effects observed in IL-10 expression and secretion were DC-SIGN dependent, we used the anti–DC-SIGN blocking antibody AZN-D1 or the Raf-1 phosphorylation inhibitor GW5074. Preincubation of DCs with AZN-D1 or GW5074 before exposure to myelin and LPS resulted in blockade of the synergistic expression and secretion of IL-10 as well as decreased T cell proliferation, likely caused by an increased frequency of anergic/suppressor T cells (Fig. 7, d–f). Moreover, the DC-SIGN-dependent up-regulation in IL-10 secretion is responsible for the decreased T cell proliferation (unpublished data). Therefore, the effect of the simultaneous stimulation with myelin and a TLR4 ligand on DCs is the triggering of an antiinflammatory response characterized by high IL-10 levels and the generation of anergic/suppressor T cells.

The loss of MOG–DC-SIGN interaction results in the activation of strong proinflammatory signals

We showed that proinflammatory stimuli induce down-regulation of fucosyltransferase transcripts (Fig. 3 d) and that myelin containing less fucosylated glycans are not recognized by DC-SIGN (Fig. 4 a). We therefore hypothesized that fucosidase-treated myelin would lack the antiinflammatory effects of healthy myelin. Indeed, fucosidase treatment reduced binding to the fucose-specific lectins LTA and UEA-I, correlating with decreased recognition by DC-SIGN (Fig. 8 a). Furthermore, exposure of DCs to fucosidase-treated myelin resulted in a lack of synergistic effect on the LPS-mediated expression (Fig. 8 b) and secretion (Fig. 8 c) of IL-10 and abrogated the myelin-induced decrease in T cell proliferation observed in the anergy/T reg assay (Fig. 8 d). These data demonstrate that the glycan-dependent interaction of myelin with DC-SIGN is necessary for the antiinflammatory effects triggered by myelin on DCs.

Interestingly, LPS-treated My^{Lo} DCs expressed very low levels of IL-10, much lower than LPS-treated DCs. We therefore investigated whether any proinflammatory pathways might be activated in these cells. Th_{17} responses have been demonstrated to be crucial in the development of MS and experimental autoimmune encephalomyelitis (Becher and Segal, 2011). Because Th_{17} cells are dependent on IL-1β for their development (van Beelen et al., 2007), we explored whether the inflammasome, which is necessary for the secretion of bioactive IL-1β (Martinon et al., 2002), was activated in My^{Lo}

FACS. Myelin uptake defined two DC populations, My^{Hi} and My^{Lo}, which were subsequently stained for MHC-II (green) and investigated by confocal microscopy (blue, myelin). Data are representative of three independent experiments. (c) DCs were exposed to atto633-labeled myelin (10 µg/ml) for 1 h and the internalization of myelin in My^{Hi} DCs was determined by imaging flow cytometry. As control, DCs incubated at 4 or 37°C with the DC-SIGN–blocking antibody AZN-D1 (10 µg/ml) were used. Data are based on at least 5,000 cells. Results are representative of three independent experiments. (d) DCs were exposed to atto633-labeled myelin (10 µg/ml) for 5 min, stained for DC-SIGN with the CSRD antibody, and tested for co-localization by imaging flow cytometry. Data are based on at least 5,000 cells. Results are representative of three independent experiments. (e) DCs were exposed to atto633-labeled myelin (10 µg/ml) for 1 h, stained for the lysosomal marker LAMP-1, and tested for colocalization by imaging flow cytometry. As control, DCs incubated at 4 or 37°C with AZN-D1 (10 µg/ml) were used. Data are based on at least 5,000 cells. Results are representative of three independent experiments. (f) DCs were incubated with atto633-labeled myelin (10 µg/ml) for 1 h in the presence or absence of LPS (10 ng/ml) and acquired by imaging flow cytometry. A mask was designed to detect myelin particles and the number of myelin particles per cell was counted. Data are based on at least 5,000 cells. Results are representative of three independent experiments. (g) Representative images demonstrating the co-localization of myelin with LAMP-1 as described in e.

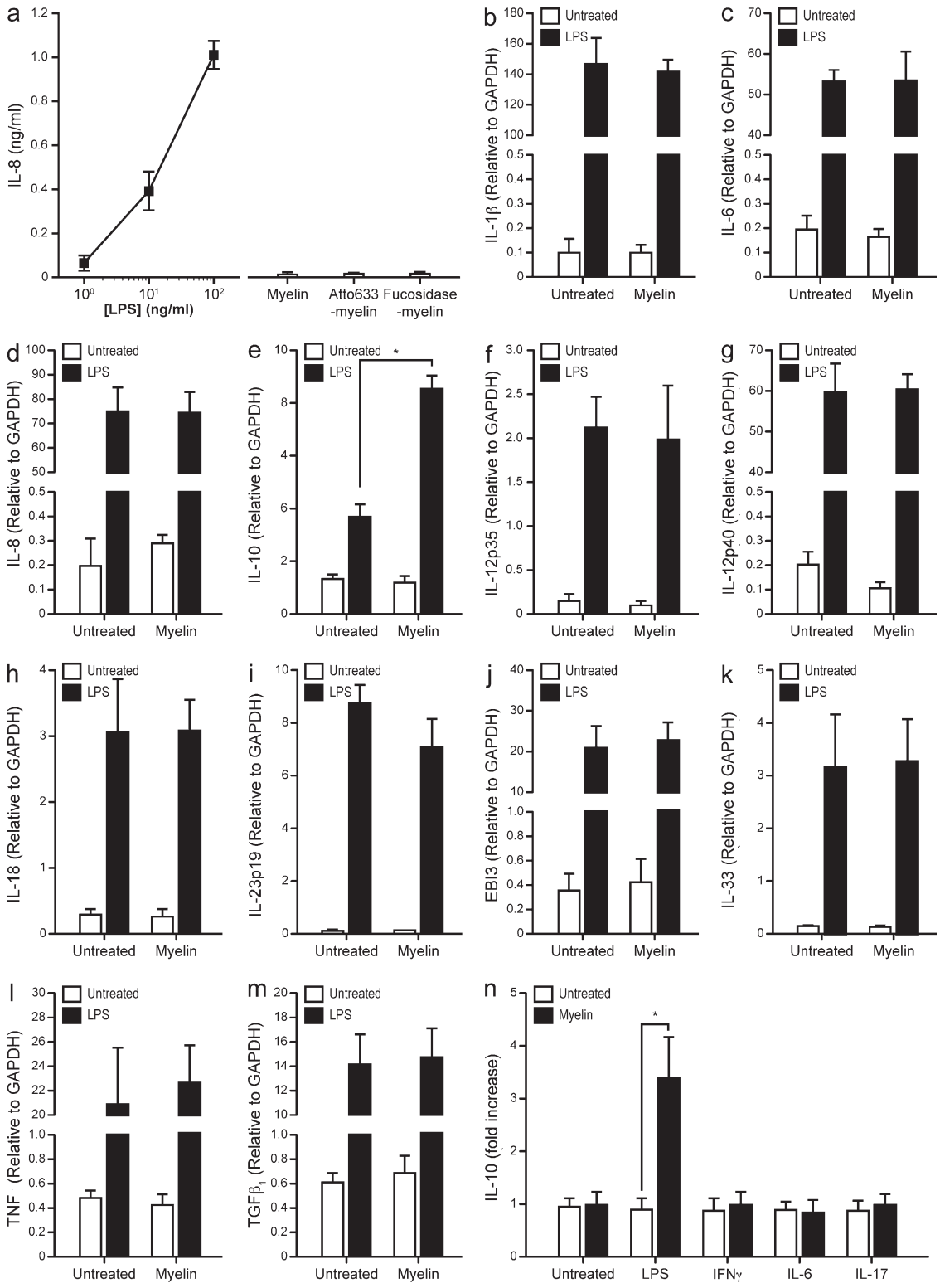

Figure 5. Myelin enhances the LPS-mediated expression of IL-10 by DCs. (a) HEK-TLR4 cells were exposed to different preparations of myelin (10 µg/ml) and assayed for IL-8 production by ELISA. A titration of LPS was used as positive control. Data are shown as the mean ± SD ($n = 3$ independent experiments). (b–m) DCs were exposed to myelin (10 µg/ml) with or without LPS (10 ng/ml) for 6 h and analyzed by real-time PCR for the expression of IL-1β (b), IL-6 (c), IL-8 (d), IL-10 (e), IL-12p35 (f), IL-12p40 (g), IL-18 (h), IL-23p19 (i), EBI3 (j), IL-33 (k), TNF (l), and TGFβ (m). *, $P \leq 0.05$ (Mann-Whitney *U* test). Data are shown as the mean the mean ± SD ($n = 7$ independent experiments). (n), DCs were exposed to myelin (10 µg/ml) with or without LPS (10 ng/ml), IFNγ (1,000 IU/ml), IL-6 (100 IU/ml), or IL-17 (100 IU/ml) for 6 h. The expression levels of IL-10 were determined by real time PCR. *, $P \leq 0.05$ (Mann-Whitney *U* test). Data are presented as the mean ± SD of the fold increase versus the corresponding stimulus ($n = 3$ independent experiments).

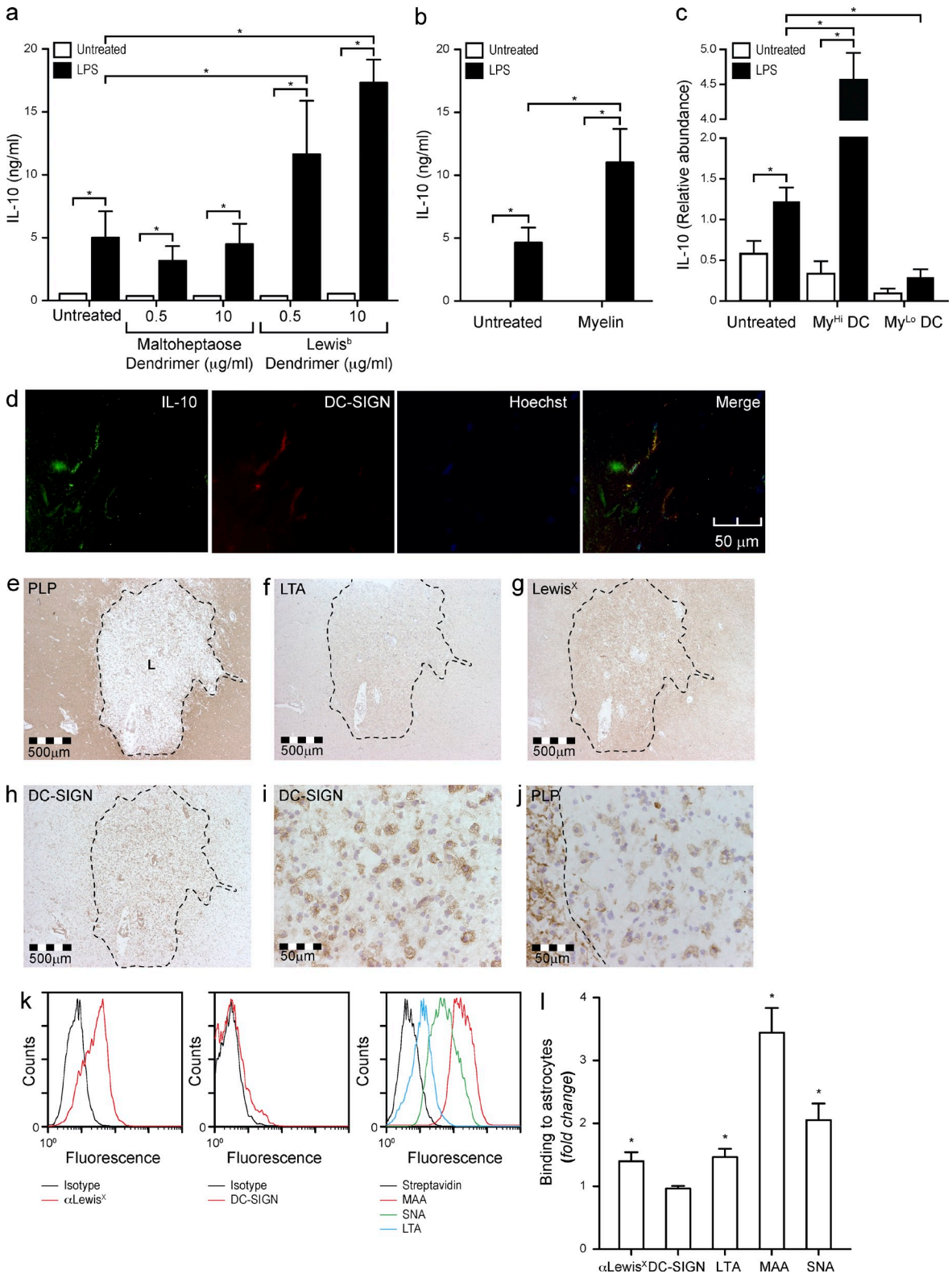

Figure 6. Simultaneous DC-SIGN and TLR4 triggering enhances IL-10 production. (a) DCs were incubated overnight with Lewis^b-containing glycodendrimers (10 μg/ml) or a mock control (maltoheptaose dendrimer, 10 μg/ml) in the presence or absence of LPS (10 ng/ml). Supernatants were assayed for IL-10 secretion by ELISA. *, $P \leq 0.05$ (Mann-Whitney *U* test). Data are shown as the mean ± SD ($n = 6$ independent experiments). (b) DCs were incubated overnight with myelin (10 μg/ml) with or without LPS (10 ng/ml). Supernatants were harvested and assayed for IL-10 secretion by ELISA. *, $P \leq 0.05$ (Mann-Whitney *U* test). Data are shown as the mean ± SD ($n = 6$ independent experiments). (c) DCs were incubated for 6 h with atto633-labeled myelin

DCs. Using a fluorescently labeled caspase-1 inhibitor, we tested whether inflammasomes were activated in DCs exposed to atto633-labeled myelin and LPS. Interestingly, only My^{Lo} DCs showed activation of caspase-1, which was enhanced by co-incubation with LPS (Fig. 8 e). In agreement with these results, My^{Lo} DCs did not reduce T cell proliferation in our anergy/T reg cell assay; on the contrary, they increased T cell proliferation in the secondary MLR (Fig. 8 f). Finally, we investigated the effect of pulsing DCs with myelin and LPS in a Th_{17} assay. Indeed, the combination of myelin and LPS resulted in the induction of IL-17A secretion by T cells (Fig. 8 g) and the up-regulation of the Th_{17}-associated transcription factor RORC (Fig. 8 h). These data demonstrate that in the absence of DC-SIGN recognition, small myelin particles induce a proinflammatory response that is characterized by the activation of the inflammasome, increased T cell proliferation, and polarization toward a Th_{17}-prone phenotype; a hallmark of autoimmune inflammation in MS.

DISCUSSION

We show here that CNS myelin interacts with APCs present in the brain and/or draining LNs through the interaction of MOG glycans with DC-SIGN, inducing an antiinflammatory/regulatory function. As the MOG–DC-SIGN interaction is glycosylation dependent, we postulate that the steady-state glycosylation of MOG is essential for the control of immune homeostasis in the human brain. Glycosylation is a tightly regulated and complex posttranslational modification that is fundamental in the modulation of the activities and functions of glycoproteins in biological systems. Our data demonstrates that changes in the glycosylation machinery of oligodendrocytes upon exposure to inflammatory mediators results in a decrease in the expression of DC-SIGN–binding glycans on myelin, which was confirmed to take place in active MS lesions. We present here a thorough characterization of the *N*-glycome of human myelin showing that the most abundant glycans on human healthy myelin are immature and (poly)-fucosylated biantennary *N*-glycans. Immature *N*-glycans are typically found within the ER and are only expressed in mature glycoproteins as a sign of ER stress. Remarkably, we found that (poly)fucosylated *N*-glycans are the most abundant mature form of *N*-glycans. Besides their well-known implications in blood groups, leukocyte adhesion, and embryogenesis, fucosylated glycans have gained much attention in the field of immunology as ligands for CLRs, particularly DC-SIGN. The presentation of several fucoses in the branches of *N*-glycans provides the opportunity for high avidity interactions that are essential for an efficient interaction of DC-SIGN with its ligands, and may contribute to increased recruitment of signaling molecules (Dam and Brewer, 2010).

We have focused our study on MOG, which despite its low abundance in CNS myelin is the dominant ligand of DC-SIGN in healthy human myelin. The glycan species identified on MOG carry one or two fucoses per branch, therefore providing the necessary avidity needed for proper interaction with DC-SIGN. Avidity may be increased at different levels: by the occurrence of MOG as a homodimer (Clements et al., 2003) and its accumulation in lipid rafts (Kim and Pfeiffer, 1999). This was clearly observed by the accumulation of MOG on large myelin particles, which, due to their size, are the only ones able to carry lipid rafts on the surface (Fan et al., 2010). Consistently we observed that only large myelin particles interacted with DC-SIGN. Le^b glycodendrimers mimicked the effect of myelin on DC-SIGN–expressing APCs, reinforcing the idea that ligand multivalency is essential for DC-SIGN function.

The vast majority of the general population does not develop autoimmune attacks against myelin. However, autoreactive T cells and antibodies specific for myelin constituents have been found in both MS and healthy patients. Therefore, mechanisms that prevent autoimmunity must exist in healthy individuals. These mechanisms are likely to work by preventing the activation and proliferation of autoreactive T cells. To date, our knowledge of these mechanisms remains limited. In particular, microglia have been reported to play a role in the regulation of homeostasis within the healthy CNS by removing cell debris. While performing this task, activation of microglia is prevented to maintain an antiinflammatory/immunosuppressive milieu. We postulate that the resting state of microglia within the healthy CNS white matter is secured by the interaction of DC-SIGN with glycosylated myelin, and MOG in particular. This interaction is likely to occur in the brain parenchyma, where DC-SIGN expression is abundant and seems to be closely associated to its ligand on myelin, as indicated by the difference in staining with AZN-D1 (a blocking antibody) and other nonblocking anti–DC-SIGN antibodies (CSRD, DC-4, and DC-28). Interaction of DC-SIGN with myelin via MOG relays an antiinflammatory signal that results in the induction of anergic/suppressive T cells. Microglia triggered via DC-SIGN may therefore contribute to the intracerebral homeostatic control of CNS-infiltrating T cells.

(10 µg/ml) in the presence or absence of LPS (10 ng/ml). DCs were then sorted according to the amount of myelin ingested into My^{Hi} and My^{Lo} DCs and lysed for mRNA isolation. The expression levels of IL-10 were determined by real-time PCR. *, $P \leq 0.05$ (Mann-Whitney *U* test). Data are shown as the mean ± SD ($n = 3$ independent experiments). (d) Frozen healthy human brain sections were stained for DC-SIGN and IL-10 and imaged by confocal microscopy (representative of $n = 3$ donors). (e–j) Consecutive brain sections from a MS patient were stained with for PLP, fucosylated glycans (LTA, αLe^X), and DC-SIGN and imaged by standard microscopy (representative of 7 donors). The MS lesion (L) is highlighted with a dotted line. (k) Primary human astrocytes were stained for $Lewis^X$, and the binding of soluble DC-SIGN and the lectins MAA, SNA, and LTA was investigated by FACS (representative of three experiments). (l) Primary human astrocytes were cultured in the presence of TNF (100 IU/ml) and IFN-γ (1,000 IU/ml) for 48 h. The expression of $Lewis^X$ and the binding of soluble DC-SIGN and the lectins LTA, MAA, and SNA was addressed by FACS. *, $P \leq 0.05$ (Mann-Whitney *U* test). Data are shown as the mean ± SD of the fold increase versus the untreated sample ($n = 3$ experiments).

In fact, IL-10 expression was found on DC-SIGN$^+$ cells within the brain, strongly supporting the existence of an antiinflammatory circuit associated with DC-SIGN engagement in the healthy human brain. Concomitantly, myelin antigens may encounter DC-SIGN$^+$ cells in the cervical LNs, where DC-SIGN$^+$ DC present antigen to T cells to activate or inhibit autoreactive T cells. We have previously described these DC-SIGN$^+$ cells in the outer zone of the paracortical areas of the LNs, where antigen capture takes place, and where myelin antigens that arrive via the lymph are often found (de Vos et al., 2002; Fabriek et al., 2005b), also in the presence of antiinflammatory cytokines (van Zwam et al., 2009). Interaction of these DC-SIGN$^+$ cells with myelin-specific autoreactive T cells could set the stage for the induction of anergy or the maintenance of memory T reg cells.

It has been established in a variety of studies that the engagement of DC-SIGN with its ligands relays inhibitory signals to DCs, which keeps them in an immature/tolerogenic state. Pathogens such as *M. tuberculosis*, HIV-1, or *C. albicans* seem to have hijacked this homeostatic mechanism via DC-SIGN to

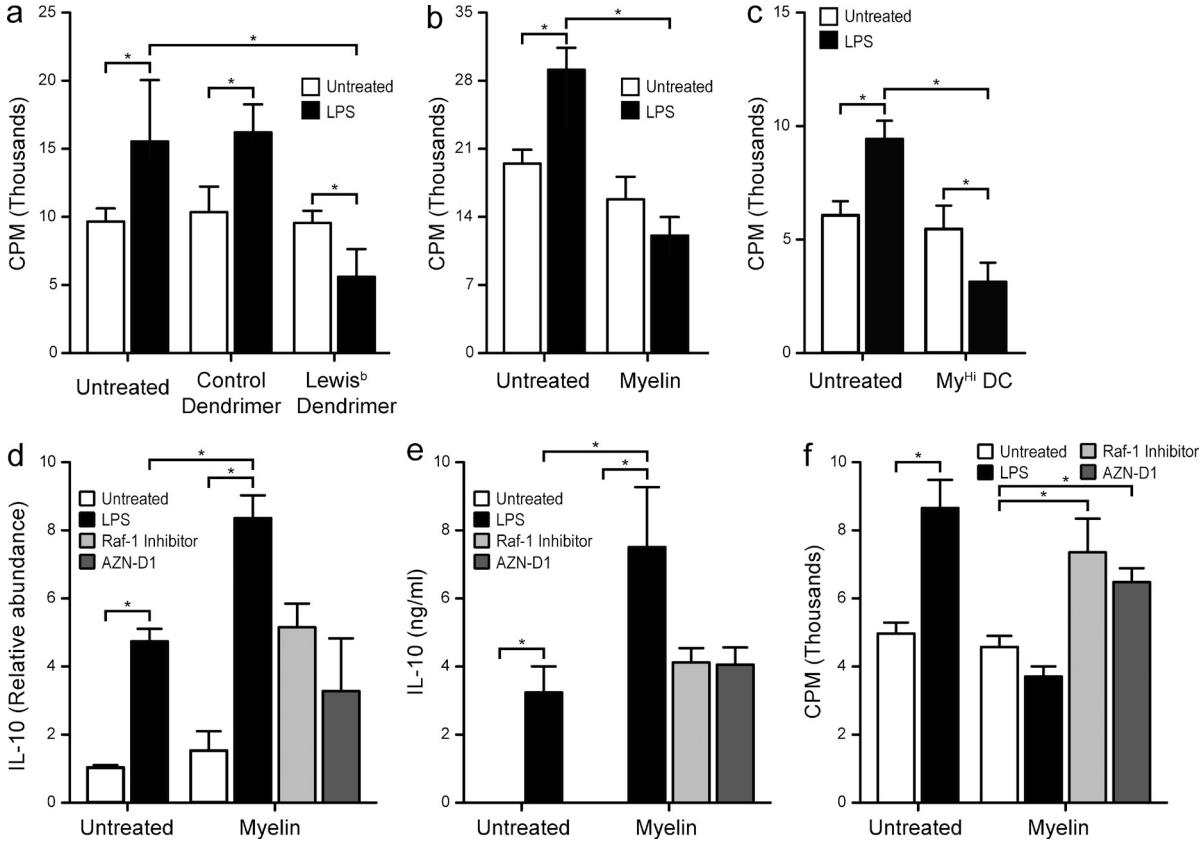

Figure 7. Simultaneous DC-SIGN and TLR4 triggering decreases allogeneic T cell proliferation. (a) DCs were pulsed with Lewis^b-containing glycodendrimers (10 µg/ml) or a mock control (maltoheptaose dendrimer, 10 µg/ml) in the presence or absence of LPS (10 ng/ml) and exposed to allogeneic naive CD4$^+$ T cells. T cells were allowed to rest, and then restimulated with LPS-matured DCs. T cell proliferation was measured by ^{3}[H]thymidine incorporation. *, $P \leq 0.05$ (Mann-Whitney *U* test). Data are shown as the mean ± SD ($n = 5$ independent experiments). (b) DCs were pulsed with myelin (10 µg/ml) in the presence or absence of LPS (10 ng/ml) and exposed to allogeneic naive CD4$^+$ T cells. T cells were allowed to rest, and then restimulated with LPS-matured DCs. T cell proliferation was measured by ^{3}[H]thymidine incorporation. *, $P \leq 0.05$ (Mann-Whitney *U* test). Data are shown as the mean ± SD ($n = 5$ independent experiments). (c) DCs were pulsed with atto633-labeled myelin (10 µg/ml) in the presence or absence of LPS (10 ng/ml) for 1 h and sorted according to their myelin content. My^{Hi} DCs were exposed to allogeneic naive CD4$^+$ T cells. T cells were allowed to rest and then restimulated with LPS-matured DCs. T cell proliferation was measured by ^{3}[H]thymidine incorporation. *, $P \leq 0.05$ (Mann-Whitney *U* test). Data are shown as the mean ± SD ($n = 3$ independent experiments). Only 1:25 DC/T cell ratios are shown; 1:50, 1:100, and 1:200 ratios showed essentially the same trend. (d) DCs were incubated 6 h with myelin (10 µg/ml) in the presence or absence of LPS (10 ng/ml) and the Raf-1 kinase inhibitor GW5074 (20 µM) or the blocking anti–DC-SIGN antibody AZN-D1 (20 µg/ml). DCs were then lysed for mRNA isolation and the expression levels of IL-10 were assayed by real time PCR. *, $P \leq 0.05$ (Mann-Whitney *U* test). Data are shown as the mean ± SD ($n = 3$ independent experiments). (e) DCs were incubated for 18 h with myelin (10 µg/ml) in the presence or absence of LPS (10 ng/ml) and the Raf-1 kinase inhibitor GW5074 (20 µM) or the blocking anti–DC-SIGN antibody AZN-D1 (20 µg/ml). Supernatants were harvested and assayed for IL-10 secretion by ELISA. *, $P \leq 0.05$ (Mann-Whitney *U* test). Data are shown as the mean ± SD ($n = 3$ independent experiments). (f) DCs were pulsed with myelin (10 µg/ml) in the presence or absence of LPS (10 ng/ml) and the Raf-1 kinase inhibitor GW5074 (20 µM) or the blocking anti–DC-SIGN antibody AZN-D1 (20 µg/ml), and exposed to allogeneic naive CD4$^+$ T cells. T cells were allowed to rest and then restimulated with LPS-matured DCs. T cell proliferation was measured by ^{3}[H]thymidine incorporation. *, $P \leq 0.05$ (Mann-Whitney *U* test). Data are shown as the mean ± SD ($n = 5$ independent experiments). Only 1:25 DC/T cell ratios are shown; 1:50, 1:100, and 1:200 ratios showed essentially the same trend.

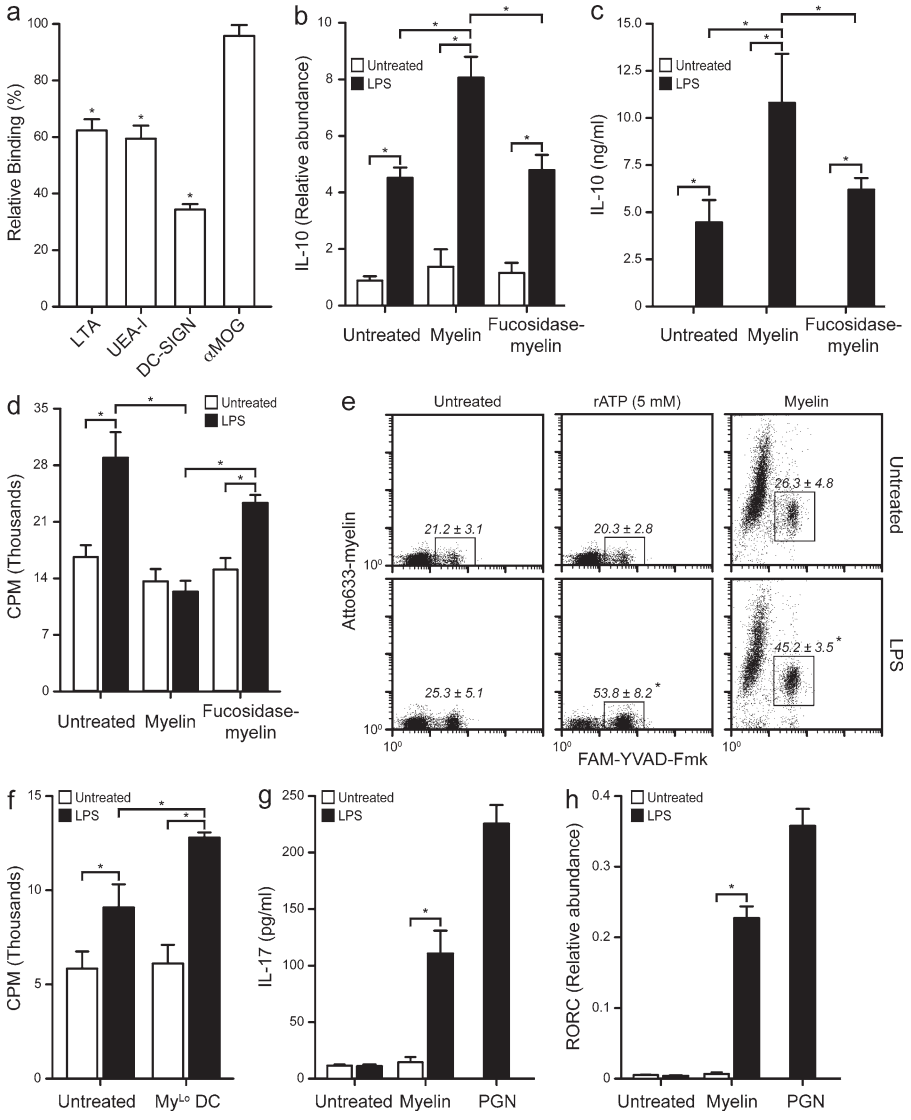

Figure 8. Defucosylated or small myelin particles are proinflammatory. (a) Myelin was defucosylated using bovine kidney α(1–2, 3, 4, 6)-Fucosidase. Defucosylation was verified by assaying the binding of the fucose specific plant lectins *Lotus tetragonolobus* (LTA) and *Ulex europaeus* (UEA-I) agglutinins, as well as the binding of recombinant DC-SIGN and the presence of MOG using the Z12 antibody on myelin (2 µg/ml) coated plates. (b) DCs were incubated 6 h with myelin (10 µg/ml) or defucosylated myelin (10 µg/ml) in the presence or absence of LPS (10 ng/ml). DCs were then lysed for mRNA isolation and the expression levels of IL-10 assayed by real-time PCR. *, $P \leq 0.05$ (Mann-Whitney *U* test). Data are shown as the mean ± SD ($n = 3$ independent experiments). (c) DCs were incubated 18 h with myelin (10 µg/ml) or defucosylated myelin (10 µg/ml) in the presence or absence of LPS (10 ng/ml). Supernatants were harvested and assayed for IL-10 secretion by ELISA. *, $P \leq 0.05$ (Mann-Whitney *U* test). Data are shown as the mean ± SD ($n = 3$ independent experiments). (d) DCs were pulsed with myelin (10 µg/ml) or defucosylated myelin (10 µg/ml), with or without LPS (10 ng/ml), and exposed to allogeneic naive $CD4^+$ T cells. T cells were allowed to rest and then restimulated with LPS-matured DCs. T cell proliferation was measured by ^{3}[H]thymidine incorporation. *, $P \leq 0.05$ (Mann-Whitney *U* test). Data are shown as the mean ± SD ($n = 5$ independent experiments). Only 1:25 DC/T cell ratios are shown; 1:50, 1:100, and 1:200 ratios showed essentially the same trend. (e) DCs were incubated with myelin (10 µg/ml) in the presence or absence of LPS (10 ng/ml). Caspase-1 activation was measured by FACS using the fluorescent caspase-1 inhibitor Fam-YVAD-Fmk. rATP (5 mM) was used as positive control for inflammasome activation. Representative dot plots of experiments ($n = 3$) performed in duplicate are shown. The mean ± SD of the gated regions in the three independent experiments are displayed. *, $P \leq 0.05$ (Mann-Whitney *U* test). (f) DCs were pulsed with atto633-labeled myelin (10 µg/ml) with or without LPS (10 ng/ml) for 1 h and sorted according to myelin content. My^{Lo} DCs were exposed to allogeneic naive $CD4^+$ T cells. T cells were allowed to rest and then restimulated with LPS-matured DCs. T cell proliferation was measured by ^{3}[H]thymidine incorporation. *, $P \leq 0.05$ (Mann-Whitney *U* test). Data are shown as the mean ± SD ($n = 3$ independent experiments). Only 1:25 DC:T cell ratios are shown; 1:50, 1:100, and 1:200 ratios showed essentially the same trend. (g) DCs were pulsed with myelin (10 µg/ml) overnight and co-cultured with allogeneic memory $CD4^+$ T cells. T cells were restimulated with IL-2 (10^4 IU/ml) twice over 2 wk and supernatants were assayed for IL-17 secretion by ELISA. Peptidoglycan (PGN; 10 µg/ml) was used as a positive control for Th_{17} skewing. *, $P \leq 0.05$ (Mann-Whitney *U* test). Data are shown as the mean ± SD ($n = 3$ independent experiments). (h) T cells from g were lysed and their mRNA assayed for the relative abundance of RORC. *, $P \leq 0.05$ (Mann-Whitney *U* test). Data are shown as the mean ± SD ($n = 3$ independent experiments).

avoid immune activation (Geijtenbeek and Gringhuis, 2009). Interaction of large myelin particles that are LTA^+ and MOG^{Hi} with DC-SIGN reflects the interaction of intact myelin with microglia in vivo, as lipid rafts are still intact in the large particles and support high avidity interactions with DC-SIGN. Furthermore, the mechanism of DC-SIGN activation and signaling seem to be similar to that previously described for pathogens (Gringhuis et al., 2007). On the contrary, the effect of smaller LTA^-MOG^{Lo} myelin particles may represent the release of degraded myelin during overt inflammation or injury, as oligodendrocyte exposure to inflammatory cues results in decreased expression of the fucosyltransferases involved in the synthesis of DC-SIGN ligands. Based on the findings reported here, we propose that the physiological role of DC-SIGN in the healthy CNS is to maintain immune homeostasis via the interaction with self-glycoproteins. We further speculate that defects in the glycosylation of MOG caused by glycosyltransferase polymorphisms or a dysregulation of glycosylation

or reduction of DC-SIGN expression may abrogate the capacity of the MOG–DC-SIGN axis to maintain tolerance. According to studies in a nonhuman primate (*Callithrix jacchus*) induction of T cell immunity against epitopes encompassed within the extracellular domain of MOG is essential for the induction of MS-like pathology and neurological defects (Jagessar et al., 2010). In line with this concept, recent evidence shows the importance of glycosylation and DC in the maintenance of immune homeostasis: α-mannosidase II–deficient mice are characterized by the expression of immature *N*-glycans that resemble pathogenic carbohydrate structures and trigger spontaneous autoimmunity (Green et al., 2007), and that loss of DC leads to a loss of T reg cells and, consequently, to autoimmunity (Darrasse-Jèze et al., 2009). The lack of control on microglia maturation may cause an altered response by microglia to CNS injury, resulting in the loss of peripheral tolerance to MOG and the development of CNS autoimmunity. Therefore, the reported observations not only have broad implications for the mechanisms that control peripheral tolerance, but also provide new possibilities for the development of therapeutic applications in neuroinflammation beyond MS.

MATERIALS AND METHODS

Myelin. Human CNS white matter tissue was obtained with informed consent at autopsy from three individuals without a history of neuroimmunological disease, in collaboration with the Dutch Brain Bank (Project #513). The Dutch Brain Bank obtained permission from its donors for brain autopsy and the use of tissue and clinical information for research purposes. The Dutch Brain Bank donor program has been approved by the Ethical Committee VU University Medical Center (Amsterdam, Netherlands). Myelin was isolated by homogenization and sucrose gradient centrifugation (Norton and Poduslo, 1973). Protein concentration in myelin was then assessed by the bicinchoninic acid method (Thermo Fisher Scientific) and labeled with NHS-activated Atto633 (Sigma-Aldrich). LPS content was assessed by incubation with HEK293-TLR4/MD2 co-transfectants, as previously described (Singh et al., 2009).

Glycan analysis. Before immunoprecipitation of MOG, myelin was subjected to delipidation by methanol/chloroform extraction. The pooled protein phase was then lyophilized, dissolved in a chaotropic detergent solution, and sonicated in the presence of β-mercaptoethanol. IGEPAL CA-630 was used to neutralize the chaotropic detergents before immunoprecipitation with anti-MOG (Z12)-coupled Sepharose beads. Both myelin and MOG glycans were resolved as previously described (Kalay et al., 2012). MOG was identified from the immunoprecipitate after deglycosylation by reduction, alkylation, and trypsinization of the recovered material and resolved by loading onto a reverse-phase peptide trap column and separation on a reverse-phase C18 HPLC directly coupled to a LCQ Deca XP Plus ion trap mass spectrometer equipped with a nanospray ionization source. The spray voltage was 2.0 kV and the capillary temperature was 150°C. The ion-trap collision fragmentation spectra were obtained using collision energies of 35%. Each full-scan mass spectrum was followed by three Data Dependent MS/MS spectra of the three most intense peaks. The Dynamic Exclusion feature was enabled and peptides and proteins were identified automatically by the computer program BioWorks version 3.1. Peptide identification was evaluated using the Xcorr versus Charge State filter, which accepts only peptides with Xcorr values of 2.5 for singly, doubly, or triply charged precursor ions.

Glycodendrimers. The peptide sequence CEEKSIINFEKLKEEK was prepared on an automated peptide synthesizer (MilliGen) in a 0.14-mmol scale, using the Fmoc strategy of solid-phase peptide synthesis. The peptide was coupled to generation 3 PAMAM dendrimers (Sigma-Aldrich) using 4-[2-[2-(tert-butoxycarbonylamino)ethyldisulfanyl]ethylamino]-4-oxo-butanoic acid as a linker. After coupling the glycan (Dextra) to MPBH (Thermo Fisher Scientific), the resulting compound was conjugated to the dendrimer.

Cells. Immature DCs were generated from $CD14^+$ monocytes obtained from human peripheral blood mononuclear cells isolated from buffy coats by Ficoll gradient and CD14 magnetic microbeads isolation (Miltenyi Biotec) that were cultured for 6 d in RPMI 1640 medium (Invitrogen) supplemented with 10% FCS (BioWhittaker), 2 mM L-glutamine (Life Technologies), 30 μg/ml penicillin/streptomycin (Life Technologies), and IL-4/GM-CSF (ImmunoTools; 500 and 800 U/ml, respectively). Primary glia culture was obtained with informed consent from ∼3 g of human brain tissue from an epileptic patient (for microglia culture) or from nondiseased rhesus macaques (for oligodendrocyte culture) and microglia or oligodendrocytes were obtained as previously described (de Groot et al., 2001). Primary human astrocytes were a gift from M. Mizee (VU University Medical Center, Amsterdam, Netherlands). Chinese Hamster Ovary (CHO) cells were cultured in RPMI-1640 supplemented with 10% FCS and 100 U/ml penicillin–streptomycin. The Lec12 glycosylation mutant (Patnaik et al., 2004) was derived from CHO cells and a gift from P. Stanley (Albert Einstein College of Medicine, Bronx, NY). Cells were transiently transfected with a plasmid encoding the full-length transcript of human MOG (pCDNA3.1-huMOG; a kind gift of Dr. D. Pham-Dinh, University of Paris) using Lipofectamine (Invitrogen). MO3.13 were a gift from P. Stinissen (University of Hasselt, Diepenbeek, Belgium) and were cultured, as previously described (Buntinx et al., 2003), in DMEM (Life Technologies) supplemented with 10% FCS, 50 U/ml penicillin, and 50 μg/ml streptomycin. MO3.13 cells were differentiated in DMEM without FCS, supplemented with 100 nM 4-β-phorbol 12-myristate 13-acetate (PMA; Sigma-Aldrich) after 70% confluency was reached. HEK293-TLR4/MD2 co-transfectants were grown in RPMI-1640 supplemented with 10% FCS, 10^4 U/ml penicillin, 10^4 U/ml streptomycin, 2 mM L-glutamine, and 1 mg/ml G418 (Invitrogen). For LPS content determination, a total of 10^5 cells in 100 μl RPMI were plated onto 96-well flat-bottom plates and stimulated with a titration of *E. coli* LPS. Subsequently, supernatants were analyzed for IL-8 production by ELISA according to the manufacturer's guidelines (Biosource).

FACS and sorting. All FACS data were collected on a FACSCalibur (BD) and analyzed using CellQuest Pro (BD) software. For sorting, cells were incubated with atto633-labeled myelin for 4 h at 37°C in 5% CO_2 atmosphere and sorted using the MoFlo High Speed Sorter (Dako) in 20% FCS DC culture medium by gating on high or low fluorescence with atto633-myelin. Myelin was labeled with NHS-atto633 (Sigma-Aldrich) before the experiment according to manufacturer's instructions. Autofluorescent cells were excluded. Purity and viability of the sorted samples was determined by reanalysis on the cell sorter. Sorting for My^{Hi} and My^{Lo} populations resulted in 85–90% pure populations.

Imaging FACS. Cells were acquired on the ImageStreamX (Amnis Corp.) imaging flow cytometer at 60× magnification and on the basis of their area (area = the number of pixels in an image reported in square micrometers). The minimum area for acquisition was set to 50 pixels. A minimum of 15,000 cells was acquired per sample at a flow rate ranging between 50 and 100 cells/s. At least 2,000 cells were acquired from single stained samples to allow for compensation. Compensation samples were acquired with all channels habilitated and with the bright-field illumination and the 785-nm laser switched off. A minimum of 5,000 cells from the single-stained samples were acquired with the same settings as experimental samples to control for over/under compensation. Analysis was performed using the IDEAS v5.0 software (Amnis Corp.). A compensation table was generated using the compensation macro built in the software. Single-stained samples were manually gated for accurate calculation of spectral overlap coefficients (Ortyn et al., 2006). Once the compensation table was calculated for each of the staining sets, it was applied

to the single staining samples that were acquired using the same settings as experimental samples. Proper compensation was then verified by visualizing samples in bivariate fluorescence intensity plots.

Next, a template analysis file was generated that include an area versus aspect ratio intensity plot and a gradient root mean square (RMS) histogram of one of the bright-field channels (Channels 1 and 9). Area is the number of squared microns of the cells, whereas the aspect ratio intensity index is the result of dividing the minor axis (intensity-weighted) by the major axis (intensity weighted) and describes how round or oblong an object is, but also indicates if there are doublets in a population of normally circular cells. The gradient RMS feature measures the sharpness quality of an image by detecting large changes of pixel values in the image and is useful for the selection of focused objects. The gradient RMS feature is computed using the mean gradient of a pixel normalized for variations in intensity levels. Using these features, a population of focused single cells (SC/F) was gated. This template, together with the corresponding compensation table was applied to all the experimental samples acquired. Each of the data files generated was opened and the SC/F population gated to a new compensated image file. Compensated image files for each experimental sample were then merged into the final analysis file. To calculate the internalization of DC-SIGN, a mask was designed that characterizes only the intracellular space of the cells. This mask was based on the use of the morphology feature applied to the bright-field image on channel 1, and then eroded until the membrane was left out of the mask. Because cells are gated on a certain level of focusing it is possible to assume that the image acquired represents, in all cells, a 2.5-µm cross section of the major circumference (Ortyn et al., 2007). At this location, the thickness of the membrane is similar in all cells and allows us to design a mask based exclusively on bright-field images. The intracellular mask was then used to calculate the feature internalization applied to the DC-SIGN channel. The internalization score is a log-scaled ratio of the intensity inside the cell (intracellular mask) versus the intensity of the entire cell. Cells that have internalized antigen typically have positive scores, whereas cells that show the antigen still on the membrane have negative scores. Cells with scores of ∼0 have similar amounts of antigen on the membrane and in intracellular compartments. Co-localization is calculated as the logarithmic transformation of Pearson's correlation coefficient of the localized bright spots with a radius of 3 pixels or less within the whole cell area in the two input images (bright detail similarity R3). Because the bright spots in the two images are either correlated (in the same spatial location) or uncorrelated (in different spatial locations), the correlation coefficient varies between 0 (uncorrelated) and 1 (perfect correlation). The logarithmic transformation of the correlation coefficient allows the use of a wider range for the colocalization score.

Antibodies and lectins. The following antibodies were purchased from BD: CD80-PE (L307.4, IgG1), CD86-PE (2331, IgG1), HLA A/B/C-PE (G46-2.6, IgG1), HLA DR-PE (G46.6, IgG2a), CD11c-APC (B-ly6, IgG1), CD31-FITC (M89D3, IgG2a), and DC-SIGN-FITC (CD209, 120507, IgG2b). Anti–CD83-PE (HB15a, IgG2b) was supplied by Beckman Coulter. The antibody against CD62L-FITC (LT-TD180, IgG1) was obtained from Immunotools. The antibody against PLP (plpc1, IgG2a) was purchased from AbD Serotec. The antibody against GFAP (6F2, IgG1) was obtained from Dako. The antibody against NGFR (rabbit polyclonal) was purchased from Abcam. The antibody against CD40 was provided by T.D. de Gruijl (VU University Medical Center, Amsterdam, Netherlands). The antibodies against PD-L1 and 4IBB-I were a gift from E.C. de Jong (University of Amsterdam, Amsterdam, Netherlands). The biotinylated lectins *Lotus tetragonolobus* agglutinin (LTA), *Aleuria aurantia* agglutinin (AAL), *Ulex europaeus* agglutinin I (UEA-I), *Griffonia simplicifolia* lectin-I isolectin B_4 (GSL-I Isolectin B_4), *Maackia amurensis* agglutinin (MAA), and *Sambucus nigra* agglutinin (SNA) were purchased from Vector Laboratories. Soluble DC-SIGN in the form of a human recombinant Fc chimera (IgG1) or a mouse Fc chimera (IgG2a) was obtained from our stocks. Anti-CD11b (bear 1, IgG1), anti-CD11c (Shcl3, IgG2b), AZN-D1 (IgG1), and Z12 (IgG2a) were purified from hybridoma supernatant using a protein A Sepharose FF column (GE Healthcare). Anti–DC-SIGN antibodies included two mouse mAbs (DC-4 [IgG1] and DC-28 [IgG2a]), a gift from R. Doms (University of Pennsylvania), as well as the polyclonal goat anti-sera CSRD. Biotinylated lectins were counterstained using streptavidin-HRP (Invitrogen). Alexa Fluor–conjugated antibodies were purchased from Invitrogen.

Immunohistochemistry and immunofluorescence microscopy. Brain tissue from seven human controls with nonneurological disease and seven patients with clinically diagnosed and neuropathologically confirmed secondary progressive MS was obtained at rapid autopsy and immediately frozen in liquid nitrogen (Project #513, Dutch Brain Bank). All donors, or their next of kin, had given informed consent for autopsy and use of their brain tissue for research purposes. Permission to perform autopsies, use of tissue, and for access to medical records for research purposes was received from the Ethical Committee of the VU University Medical Center (Amsterdam, Netherlands). White matter MS tissue samples were selected by postmortem MRI, as previously described (De Groot et al., 2001). For immunohistochemical stainings, 5-µm serial cryosections were air dried and fixed in acetone. Sections were blocked with normal serum before incubation with primary antibodies and subsequently incubated with the biotinylated appropriate secondary antibody. After incubating for 60 min with streptavidin–HRP complex, peroxidase labeling was visualized by 3,3-diaminobenzidine (Sigma-Aldrich). Finally, tissue sections were counterstained with hematoxylin and mounted. Between all incubation steps, the sections were extensively washed in PBS. For immunofluorescence, Alexa Fluor 488– and Alexa Fluor 594–conjugated secondary antibodies were used. Analysis was performed on a standard epifluorescence microscope (Nikon DM6000).

Confocal laser-scanning microscopy. Stained cells were allowed to adhere to poly-L-lysine–coated glass slides (Sigma-Aldrich) and mounted with antibleach reagent (Vector Laboratories). Samples were analyzed using a 63×/1.4 HCX PL APO CS oil objective on a TCS SP2 AOBS confocal microscope (Leica). Images were acquired using LCS 2.61 (Leica) and processed using ImageJ (National Institutes of Health).

Electron microscopy. Myelin particles were dried on carbon/formvar-coated copper mesh grids (Electron Microscopy Sciences) and stained by uranyl acetate (Sigma-Aldrich) in methylcellulose (Sigma-Aldrich) before analysis by transmission electron microscopy (JEOL 1010; JEOL).

Cytokine measurements. For the detection of cytokines, culture supernatants were harvested 24 h after DC activation and frozen at −80°C until analysis. Cytokines were measured by ELISA with antibody pairs for human IL-6, IL-10, TNF, IL-12p40, and IL-12p70 according to the manufacturer's instructions (eBioscience).

T reg cell/anergy induction assays (secondary MLRs). Naive $CD4^+CD45^+$ T cells were purified by negative selection (Invitrogen) and cultured with allogeneic myelin-stimulated DCs in 24-well plates for 6 d. Primed T cells were recovered, washed, and allowed to rest for 3 d in the presence of IL-7 and IL-15 (ImmunoTools). After 9 d of the primary stimulation, primed T cells were washed and restimulated by co-culturing them with LPS-activated moDC from the original donor at different ratios. After 6 d, plates were pulsed with $[^3H]$thymidine (1 µCi/well; GE Healthcare) for an additional 18 h and $[^3H]$thymidine incorporation was measured on a Betaplate 1205 liquid scintillation counter (Wallac-LKB).

DC-driven Th_{17} differentiation. Total $CD4^+$ T cells were negatively isolated from PBMCs and co-cultured with myelin-stimulated allogeneic DC. At day 3–5, rhuIL-2 (ImmunoTools) was added, and the cultures were expanded for the next 12–14 d. Cultures were refreshed once with rhuIL-2 and media at days 7–9. Expanded T cells were restimulated on day 12–14 with PMA and ionomycin (Sigma-Aldrich) for 6 h, with brefeldin A (Sigma-Aldrich) present during the last 5 h. T cells were then fixated on Cytofix/Cytoperm solution (BD) and single-cell production of IL-17 and IFN-γ was determined by intracellular staining (BD) and FACS. Additionally, IL-17 was determined in T cell supernatants using an anti–IL-17 antibody pair (ImmunoTools).

Caspase-1 activation. Caspase-1 activity was assessed with a Caspase 1 FLICA kit according to the manufacturer's instructions (Bachem).

mRNA isolation, cDNA synthesis, and real-time PCR. mRNA was isolated using an mRNA Capture kit (Roche) and cDNA was synthesized with the Reverse Transcription System kit (Promega). Real-time PCR were set up using the SYBR Green method in an ABI 7900HT sequence detection system as previously described (García-Vallejo et al., 2004).

Statistics. Statistical significance was determined by Mann-Whitney's *U* test, with P values of <0.05 considered statistically significant.

We thank S. van der Pol for support with the immunohistochemical stainings and M. Mizee for the preparation of astrocytes. This research was supported by grants from NWO (VENI 863.08.020, J.J. García-Vallejo), Longfonds (3.2.10.040, J.J. García-Vallejo) and the Dutch MS-Research Foundation (MS06-598, MS05-560, Y. van Kooyk). J.G.M. Bolscher and K. Nazmi were supported by a grant from the University of Amsterdam for research into focal point oral infections and inflammation.

The authors declare no conflicting financial interests.

Submitted: 27 September 2012
Accepted: 9 May 2014

REFERENCES

Appelmelk, B.J., I. van Die, S.J. van Vliet, C.M.J.E. Vandenbroucke-Grauls, T.B.H. Geijtenbeek, and Y. van Kooyk. 2003. Cutting edge: carbohydrate profiling identifies new pathogens that interact with dendritic cell-specific ICAM-3-grabbing nonintegrin on dendritic cells. *J. Immunol.* 170:1635–1639. http://dx.doi.org/10.4049/jimmunol.170.4.1635

Becher, B., and B.M. Segal. 2011. T(H)17 cytokines in autoimmune neuroinflammation. *Curr. Opin. Immunol.* 23:707–712. http://dx.doi.org/10.1016/j.coi.2011.08.005

Birnberg, T., L. Bar-On, A. Sapoznikov, M.L. Caton, L. Cervantes-Barragán, D. Makia, R. Krauthgamer, O. Brenner, B. Ludewig, D. Brockschnieder, et al. 2008. Lack of conventional dendritic cells is compatible with normal development and T cell homeostasis, but causes myeloid proliferative syndrome. *Immunity.* 29:986–997. http://dx.doi.org/10.1016/j.immuni.2008.10.012

Boven, L.A., M. Van Meurs, M. Van Zwam, A. Wierenga-Wolf, R.Q. Hintzen, R.G. Boot, J.M. Aerts, S. Amor, E.E. Nieuwenhuis, and J.D. Laman. 2006. Myelin-laden macrophages are anti-inflammatory, consistent with foam cells in multiple sclerosis. *Brain.* 129:517–526. http://dx.doi.org/10.1093/brain/awh707

Brynedal, B., J. Wojcik, F. Esposito, V. Debailleul, J. Yaouanq, F. Martinelli-Boneschi, G. Edan, G. Comi, J. Hillert, and H. Abderrahim. 2010. MGAT5 alters the severity of multiple sclerosis. *J. Neuroimmunol.* 220:120–124. http://dx.doi.org/10.1016/j.jneuroim.2010.01.003

Buntinx, M., J. Vanderlocht, N. Hellings, F. Vandenabeele, I. Lambrichts, J. Raus, M. Ameloot, P. Stinissen, and P. Steels. 2003. Characterization of three human oligodendroglial cell lines as a model to study oligodendrocyte injury: morphology and oligodendrocyte-specific gene expression. *J. Neurocytol.* 32:25–38. http://dx.doi.org/10.1023/A:1027324230923

Cambi, A., I. Beeren, B. Joosten, J.A. Fransen, and C.G. Figdor. 2009. The C-type lectin DC-SIGN internalizes soluble antigens and HIV-1 virions via a clathrin-dependent mechanism. *Eur. J. Immunol.* 39:1923–1928. http://dx.doi.org/10.1002/eji.200939351

Caparrós, E., P. Munoz, E. Sierra-Filardi, D. Serrano-Gómez, A. Puig-Kröger, J.L. Rodríguez-Fernández, M. Mellado, J. Sancho, M. Zubiaur, and A.L. Corbí. 2006. DC-SIGN ligation on dendritic cells results in ERK and PI3K activation and modulates cytokine production. *Blood.* 107:3950–3958. http://dx.doi.org/10.1182/blood-2005-03-1252

Clements, C.S., H.H. Reid, T. Beddoe, F.E. Tynan, M.A. Perugini, T.G. Johns, C.C.A. Bernard, and J. Rossjohn. 2003. The crystal structure of myelin oligodendrocyte glycoprotein, a key autoantigen in multiple sclerosis. *Proc. Natl. Acad. Sci. USA.* 100:11059–11064. http://dx.doi.org/10.1073/pnas.1833158100

Cong, Y., A. Konrad, N. Iqbal, R.D. Hatton, C.T. Weaver, and C.O. Elson. 2005. Generation of antigen-specific, Foxp3-expressing CD4+ regulatory T cells by inhibition of APC proteosome function. *J. Immunol.* 174:2787–2795. http://dx.doi.org/10.4049/jimmunol.174.5.2787

Dam, T.K., and C.F. Brewer. 2010. Lectins as pattern recognition molecules: the effects of epitope density in innate immunity. *Glycobiology.* 20:270–279. http://dx.doi.org/10.1093/glycob/cwp186

Darrasse-Jèze, G., S. Deroubaix, H. Mouquet, G.D. Victora, T. Eisenreich, K.-H. Yao, R.F. Masilamani, M.L. Dustin, A. Rudensky, K. Liu, and M.C. Nussenzweig. 2009. Feedback control of regulatory T cell homeostasis by dendritic cells in vivo. *J. Exp. Med.* 206:1853–1862. http://dx.doi.org/10.1084/jem.20090746

De Groot, C.J., E. Bergers, W. Kamphorst, R. Ravid, C.H. Polman, F. Barkhof, and P. van der Valk. 2001. Post-mortem MRI-guided sampling of multiple sclerosis brain lesions: increased yield of active demyelinating and (p)reactive lesions. *Brain.* 124:1635–1645. http://dx.doi.org/10.1093/brain/124.8.1635

de Groot, C.J., S. Hulshof, J.J. Hoozemans, and R. Veerhuis. 2001. Establishment of microglial cell cultures derived from postmortem human adult brain tissue: immunophenotypical and functional characterization. *Microsc. Res. Tech.* 54:34–39. http://dx.doi.org/10.1002/jemt.1118

de Vos, A.F., M. van Meurs, H.P. Brok, L.A. Boven, R.Q. Hintzen, P. van der Valk, R. Ravid, S. Rensing, L. Boon, B.A. 't Hart, and J.D. Laman. 2002. Transfer of central nervous system autoantigens and presentation in secondary lymphoid organs. *J. Immunol.* 169:5415–5423. http://dx.doi.org/10.4049/jimmunol.169.10.5415

Engering, A., T.B. Geijtenbeek, S.J. van Vliet, M. Wijers, E. van Liempt, N. Demaurex, A. Lanzavecchia, J. Fransen, C.G. Figdor, V. Piguet, and Y. van Kooyk. 2002. The dendritic cell-specific adhesion receptor DC-SIGN internalizes antigen for presentation to T cells. *J. Immunol.* 168:2118–2126. http://dx.doi.org/10.4049/jimmunol.168.5.2118

Engering, A., S.J. van Vliet, K. Hebeda, D.G. Jackson, R. Prevo, S.K. Singh, T.B.H. Geijtenbeek, H. van Krieken, and Y. van Kooyk. 2004. Dynamic populations of dendritic cell-specific ICAM-3 grabbing nonintegrin-positive immature dendritic cells and liver/lymph node-specific ICAM-3 grabbing nonintegrin-positive endothelial cells in the outer zones of the paracortex of human lymph nodes. *Am. J. Pathol.* 164:1587–1595. http://dx.doi.org/10.1016/S0002-9440(10)63717-0

Fabriek, B.O., E.S. Van Haastert, I. Galea, M.M.J. Polfliet, E.D. Döpp, M.M. Van Den Heuvel, T.K. Van Den Berg, C.J.A. De Groot, P. Van Der Valk, and C.D. Dijkstra. 2005a. CD163-positive perivascular macrophages in the human CNS express molecules for antigen recognition and presentation. *Glia.* 51:297–305. http://dx.doi.org/10.1002/glia.20208

Fabriek, B.O., J.N.P. Zwemmer, C.E. Teunissen, C.D. Dijkstra, C.H. Polman, J.D. Laman, and J.A. Castelijns. 2005b. In vivo detection of myelin proteins in cervical lymph nodes of MS patients using ultrasound-guided fine-needle aspiration cytology. *J. Neuroimmunol.* 161:190–194. http://dx.doi.org/10.1016/j.jneuroim.2004.12.018

Fan, J., M. Sammalkorpi, and M. Haataja. 2010. Formation and regulation of lipid microdomains in cell membranes: theory, modeling, and speculation. *FEBS Lett.* 584:1678–1684. http://dx.doi.org/10.1016/j.febslet.2009.10.051

Fehérvári, Z., and S. Sakaguchi. 2004. Control of Foxp3+ CD25+CD4+ regulatory cell activation and function by dendritic cells. *Int. Immunol.* 16:1769–1780. http://dx.doi.org/10.1093/intimm/dxh178

García-Vallejo, J.J., and Y. van Kooyk. 2009. Endogenous ligands for C-type lectin receptors: the true regulators of immune homeostasis. *Immunol. Rev.* 230:22–37. http://dx.doi.org/10.1111/j.1600-065X.2009.00786.x

García-Vallejo, J.J., and Y. van Kooyk. 2013. The physiological role of DC-SIGN: a tale of mice and men. *Trends Immunol.* 34:482–486. http://dx.doi.org/10.1016/j.it.2013.03.001

García-Vallejo, J.J., B. Van Het Hof, J. Robben, J.A.E. Van Wijk, I. Van Die, D.H. Joziasse, and W. Van Dijk. 2004. Approach for defining endogenous reference genes in gene expression experiments. *Anal. Biochem.* 329:293–299. http://dx.doi.org/10.1016/j.ab.2004.02.037

Geijtenbeek, T.B.H., and S.I. Gringhuis. 2009. Signalling through C-type lectin receptors: shaping immune responses. *Nat. Rev. Immunol.* 9:465–479. http://dx.doi.org/10.1038/nri2569

Geijtenbeek, T.B.H., S.J. Van Vliet, E.A. Koppel, M. Sanchez-Hernandez, C.M.J.E. Vandenbroucke-Grauls, B.J. Appelmelk, and Y. Van Kooyk.

2003. Mycobacteria target DC-SIGN to suppress dendritic cell function. *J. Exp. Med.* 197:7–17. http://dx.doi.org/10.1084/jem.20021229

Green, R.S., E.L. Stone, M. Tenno, E. Lehtonen, M.G. Farquhar, and J.D. Marth. 2007. Mammalian N-glycan branching protects against innate immune self-recognition and inflammation in autoimmune disease pathogenesis. *Immunity*. 27:308–320. http://dx.doi.org/10.1016/j.immuni.2007.06.008

Gringhuis, S.I., J. den Dunnen, M. Litjens, B. van Het Hof, Y. van Kooyk, and T.B.H. Geijtenbeek. 2007. C-type lectin DC-SIGN modulates Toll-like receptor signaling via Raf-1 kinase-dependent acetylation of transcription factor NF-kappaB. *Immunity*. 26:605–616. http://dx.doi.org/10.1016/j.immuni.2007.03.012

Gringhuis, S.I., J. den Dunnen, M. Litjens, M. van der Vlist, and T.B.H. Geijtenbeek. 2009. Carbohydrate-specific signaling through the DC-SIGN signalosome tailors immunity to *Mycobacterium tuberculosis*, HIV-1 and *Helicobacter pylori*. *Nat. Immunol.* 10:1081–1088. http://dx.doi.org/10.1038/ni.1778

Hawiger, D., K. Inaba, Y. Dorsett, M. Guo, K. Mahnke, M. Rivera, J.V. Ravetch, R.M. Steinman, and M.C. Nussenzweig. 2001. Dendritic cells induce peripheral T cell unresponsiveness under steady state conditions in vivo. *J. Exp. Med.* 194:769–779. http://dx.doi.org/10.1084/jem.194.6.769

Hoppenbrouwers, I.A., Y.S. Aulchenko, A.C. Janssens, S.V. Ramagopalan, L. Broer, M. Kayser, G.C. Ebers, B.A. Oostra, C.M. van Duijn, and R.Q. Hintzen. 2009. Replication of CD58 and CLEC16A as genome-wide significant risk genes for multiple sclerosis. *J. Hum. Genet.* 54:676–680. http://dx.doi.org/10.1038/jhg.2009.96

Husain, S., C. Yildirim-Toruner, J.P. Rubio, J. Field, M. Schwalb, S. Cook, M. Devoto, and E. Vitale; Southern MS Genetics Consortium. 2008. Variants of ST8SIA1 are associated with risk of developing multiple sclerosis. *PLoS ONE*. 3:e2653. http://dx.doi.org/10.1371/journal.pone.0002653

Jagessar, S.A., Y.S. Kap, N. Heijmans, N. van Driel, L. van Straalen, J.J. Bajramovic, H.P.M. Brok, E.L.A. Blezer, J. Bauer, J.D. Laman, and B.A. 't Hart. 2010. Induction of progressive demyelinating autoimmune encephalomyelitis in common marmoset monkeys using MOG34-56 peptide in incomplete freund adjuvant. *J. Neuropathol. Exp. Neurol.* 69:372–385. http://dx.doi.org/10.1097/NEN.0b013e3181d5d053

Kalay, H., M. Ambrosini, P.H.C. van Berkel, P.W.H.I. Parren, Y. van Kooyk, and J.J. García Vallejo. 2012. Online nanoliquid chromatography-mass spectrometry and nanofluorescence detection for high-resolution quantitative N-glycan analysis. *Anal. Biochem.* 423:153–162. http://dx.doi.org/10.1016/j.ab.2012.01.015

Kim, T., and S.E. Pfeiffer. 1999. Myelin glycosphingolipid/cholesterol-enriched microdomains selectively sequester the non-compact myelin proteins CNP and MOG. *J. Neurocytol.* 28:281–293. http://dx.doi.org/10.1023/A:1007001427597

Lambert, C., J. Desbarats, N. Arbour, J.A. Hall, A. Olivier, A. Bar-Or, and J.P. Antel. 2008. Dendritic cell differentiation signals induce anti-inflammatory properties in human adult microglia. *J. Immunol.* 181:8288–8297. http://dx.doi.org/10.4049/jimmunol.181.12.8288

Latz, E., A. Visintin, E. Lien, K.A. Fitzgerald, B.G. Monks, E.A. Kurt-Jones, D.T. Golenbock, and T. Espevik. 2002. Lipopolysaccharide rapidly traffics to and from the Golgi apparatus with the toll-like receptor 4-MD-2-CD14 complex in a process that is distinct from the initiation of signal transduction. *J. Biol. Chem.* 277:47834–47843. http://dx.doi.org/10.1074/jbc.M207873200

Liu, K., T. Iyoda, M. Saternus, Y. Kimura, K. Inaba, and R.M. Steinman. 2002. Immune tolerance after delivery of dying cells to dendritic cells in situ. *J. Exp. Med.* 196:1091–1097. http://dx.doi.org/10.1084/jem.20021215

Martinon, F., K. Burns, and J. Tschopp. 2002. The inflammasome: a molecular platform triggering activation of inflammatory caspases and processing of proIL-beta. *Mol. Cell.* 10:417–426. http://dx.doi.org/10.1016/S1097-2765(02)00599-3

Nonaka, M., B.Y. Ma, R. Murai, N. Nakamura, M. Baba, N. Kawasaki, K. Hodohara, S. Asano, and T. Kawasaki. 2008. Glycosylation-dependent interactions of C-type lectin DC-SIGN with colorectal tumor-associated Lewis glycans impair the function and differentiation of monocyte-derived dendritic cells. *J. Immunol.* 180:3347–3356. http://dx.doi.org/10.4049/jimmunol.180.5.3347

North, S.J., H.-H. Huang, S. Sundaram, J. Jang-Lee, A.T. Etienne, A. Trollope, S. Chalabi, A. Dell, P. Stanley, and S.M. Haslam. 2010. Glycomics profiling of Chinese hamster ovary cell glycosylation mutants reveals N-glycans of a novel size and complexity. *J. Biol. Chem.* 285:5759–5775. http://dx.doi.org/10.1074/jbc.M109.068353

Norton, W.T., and S.E. Poduslo. 1973. Myelination in rat brain: method of myelin isolation. *J. Neurochem.* 21:749–757. http://dx.doi.org/10.1111/j.1471-4159.1973.tb07519.x

Ohnmacht, C., A. Pullner, S.B.S. King, I. Drexler, S. Meier, T. Brocker, and D. Voehringer. 2009. Constitutive ablation of dendritic cells breaks self-tolerance of CD4 T cells and results in spontaneous fatal autoimmunity. *J. Exp. Med.* 206:549–559. http://dx.doi.org/10.1084/jem.20082394

Olson, J.K., and S.D. Miller. 2004. Microglia initiate central nervous system innate and adaptive immune responses through multiple TLRs. *J. Immunol.* 173:3916–3924. http://dx.doi.org/10.4049/jimmunol.173.6.3916

Ortyn, W.E., B.E. Hall, T.C. George, K. Frost, D.A. Basiji, D.J. Perry, C.A. Zimmerman, D. Coder, and P.J. Morrissey. 2006. Sensitivity measurement and compensation in spectral imaging. *Cytometry A*. 69:852–862. http://dx.doi.org/10.1002/cyto.a.20306

Ortyn, W.E., D.J. Perry, V. Venkatachalam, L. Liang, B.E. Hall, K. Frost, and D.A. Basiji. 2007. Extended depth of field imaging for high speed cell analysis. *Cytometry A*. 71:215–231. http://dx.doi.org/10.1002/cyto.a.20370

Park, C.G., K. Takahara, E. Umemoto, Y. Yashima, K. Matsubara, Y. Matsuda, B.E. Clausen, K. Inaba, and R.M. Steinman. 2001. Five mouse homologues of the human dendritic cell C-type lectin, DC-SIGN. *Int. Immunol.* 13:1283–1290. http://dx.doi.org/10.1093/intimm/13.10.1283

Patnaik, S.K., B. Potvin, and P. Stanley. 2004. LEC12 and LEC29 gain-of-function Chinese hamster ovary mutants reveal mechanisms for regulating VIM-2 antigen synthesis and E-selectin binding. *J. Biol. Chem.* 279:49716–49726. http://dx.doi.org/10.1074/jbc.M408755200

Powlesland, A.S., E.M. Ward, S.K. Sadhu, Y. Guo, M.E. Taylor, and K. Drickamer. 2006. Widely divergent biochemical properties of the complete set of mouse DC-SIGN-related proteins. *J. Biol. Chem.* 281:20440–20449. http://dx.doi.org/10.1074/jbc.M601925200

Rappocciolo, G., H.R. Hensler, M. Jais, T.A. Reinhart, A. Pegu, F.J. Jenkins, and C.R. Rinaldo. 2008. Human herpesvirus 8 infects and replicates in primary cultures of activated B lymphocytes through DC-SIGN. *J. Virol.* 82:4793–4806. http://dx.doi.org/10.1128/JVI.01587-07

Serafini, B., B. Rosicarelli, R. Magliozzi, E. Stigliano, E. Capello, G.L. Mancardi, and F. Aloisi. 2006. Dendritic cells in multiple sclerosis lesions: maturation stage, myelin uptake, and interaction with proliferating T cells. *J. Neuropathol. Exp. Neurol.* 65:124–141.

Simons, K., and W.L.C. Vaz. 2004. Model systems, lipid rafts, and cell membranes. *Annu. Rev. Biophys. Biomol. Struct.* 33:269–295. http://dx.doi.org/10.1146/annurev.biophys.32.110601.141803

Singh, S.K., J. Stephani, M. Schaefer, H. Kalay, J.J. García-Vallejo, J. den Haan, E. Saeland, T. Sparwasser, and Y. van Kooyk. 2009. Targeting glycan modified OVA to murine DC-SIGN transgenic dendritic cells enhances MHC class I and II presentation. *Mol. Immunol.* 47:164–174. http://dx.doi.org/10.1016/j.molimm.2009.09.026

Smith, P.A., N. Heijmans, B. Ouwerling, E.C. Breij, N. Evans, J.M. van Noort, A.C. Plomp, C. Delarasse, B. 't Hart, D. Pham-Dinh, and S. Amor. 2005. Native myelin oligodendrocyte glycoprotein promotes severe chronic neurological disease and demyelination in Biozzi ABH mice. *Eur. J. Immunol.* 35:1311–1319. http://dx.doi.org/10.1002/eji.200425842

Sofroniew, M.V. 2009. Molecular dissection of reactive astrogliosis and glial scar formation. *Trends Neurosci.* 32:638–647. http://dx.doi.org/10.1016/j.tins.2009.08.002

Soilleux, E.J., L.S. Morris, G. Leslie, J. Chehimi, Q. Luo, E. Levroney, J. Trowsdale, L.J. Montaner, R.W. Doms, D. Weissman, et al. 2002. Constitutive and induced expression of DC-SIGN on dendritic cell and macrophage subpopulations in situ and in vitro. *J. Leukoc. Biol.* 71:445–457.

van Beelen, A.J., Z. Zelinkova, E.W. Taanman-Kueter, F.J. Muller, D.W. Hommes, S.A.J. Zaat, M.L. Kapsenberg, and E.C. de Jong. 2007. Stimulation of the intracellular bacterial sensor NOD2 programs dendritic cells to promote interleukin-17 production in human memory T cells. *Immunity*. 27:660–669. http://dx.doi.org/10.1016/j.immuni.2007.08.013

van Gisbergen, K.P.J.M., C.A. Aarnoudse, G.A. Meijer, T.B.H. Geijtenbeek, and Y. van Kooyk. 2005. Dendritic cells recognize tumor-specific glycosylation of carcinoembryonic antigen on colorectal cancer cells through dendritic cell-specific intercellular adhesion molecule-3-grabbing nonintegrin. *Cancer Res.* 65:5935–5944. http://dx.doi.org/10.1158/0008-5472.CAN-04-4140

van Kooyk, Y., and T.B.H. Geijtenbeek. 2003. DC-SIGN: escape mechanism for pathogens. *Nat. Rev. Immunol.* 3:697–709. http://dx.doi.org/10.1038/nri1182

van Zwam, M., R. Huizinga, M.-J. Melief, A.F. Wierenga-Wolf, M. van Meurs, J.S. Voerman, K.P.H. Biber, H.W.G.M. Boddeke, U.E. Höpken, C. Meisel, et al. 2009. Brain antigens in functionally distinct antigen-presenting cell populations in cervical lymph nodes in MS and EAE. *J. Mol. Med.* 87:273–286. http://dx.doi.org/10.1007/s00109-008-0421-4

Wang, S.-F., J.C. Huang, Y.-M. Lee, S.-J. Liu, Y.-J. Chan, Y.-P. Chau, P. Chong, and Y.M.A. Chen. 2008. DC-SIGN mediates avian H5N1 influenza virus infection in cis and in trans. *Biochem. Biophys. Res. Commun.* 373:561–566. http://dx.doi.org/10.1016/j.bbrc.2008.06.078